Protein production dynamics and physiological adaptation of recombinant *Komagataella phaffii* at near-zero growth rates

Corinna Rebnegger[1,2,3], Benjamin L. Coltman[1,2], Viktoria Kowarz[1,2], David A. Peña[2], Axel Mentler[4], Christina Troyer[5], Stephan Hann[5], Harald Schöny[6], Gunda Koellensperger[6,7], Diethard Mattanovich[1,2,3] and Brigitte Gasser[1,2,3*]

Abstract

Background Specific productivity (q_P) in yeast correlates with growth, typically peaking at intermediate or maximum specific growth rates (μ). Understanding the factors limiting productivity at extremely low μ might reveal decoupling strategies, but knowledge of production dynamics and physiology in such conditions is scarce. Retentostats, a type of continuous cultivation, enable the well-controlled transition to near-zero μ through the combined retention of biomass and limited substrate supply. Recombinant *Komagataella phaffii* (syn *Pichia pastoris*) secreting a bivalent single domain antibody (VHH) was cultivated in aerobic, glucose-limited retentostats to investigate recombinant protein production dynamics and broaden our understanding of relevant physiological adaptations at near-zero growth conditions.

Results By the end of the retentostat cultivation, doubling times of approx. two months were reached, corresponding to μ = 0.00047 h^{-1}. Despite these extremely slow growth rates, the proportion of viable cells remained high, and de novo synthesis and secretion of the VHH were observed. The average q_P at the end of the retentostat was estimated at 0.019 mg g^{-1} h^{-1}. Transcriptomics indicated that genes involved in protein biosynthesis were only moderately downregulated towards zero growth, while secretory pathway genes were mostly regulated in a manner seemingly detrimental to protein secretion. Adaptation to near-zero growth conditions of recombinant *K. phaffii* resulted in significant changes in the total protein, RNA, DNA and lipid content, and lipidomics revealed a complex adaptation pattern regarding the lipid class composition. The higher abundance of storage lipids as well as storage carbohydrates indicates that the cells are preparing for long-term survival.

Conclusions In conclusion, retentostat cultivation proved to be a valuable tool to identify potential engineering targets to decouple growth and protein production and gain important insights into the physiological adaptation of *K. phaffii* to near-zero growth conditions.

*Correspondence:
Brigitte Gasser
brigitte.gasser@boku.ac.at
Full list of author information is available at the end of the article

Introduction

The market for biopharmaceutical proteins is valued at US \$271 billion for 2021 and is expected to continue to grow in the upcoming years [1]. For the production of biopharmaceutical proteins and other recombinant proteins employed in medicine, research, and industry, budding yeasts like methylotrophic *Komagataella phaffii* (*Pichia pastoris*) have gained increasing popularity. They combine benefits of prokaryotic expression systems, including ease of genetic manipulation, short strain development times, fast growth to high cell densities, and minimal media requirements, with the ability to perform most post-translational modifications and secrete the recombinant protein into the supernatant, facilitating downstream processing [2–4].

In *K. phaffii* and other yeasts, the production of heterologous proteins is generally growth-rate-dependent, typically peaking at intermediate or near maximum specific growth rates (μ) [5, 6]. However, the respective relationship between the biomass-specific product formation rate (q_P) and μ for a certain recombinant protein can vary greatly according to the regulatory properties of the respective promoter selected for controlling recombinant gene transcription (as well as culture conditions) and needs to be determined empirically. Multiple omics studies have demonstrated that variations in μ are readily reflected by alterations in the transcriptome, proteome, and metabolome of yeasts [7–12]. The main trend of adaptations appears to be well-conserved among different yeast species. These include the upregulation of essential genes with a role in gene transcription and protein biosynthesis at higher growth rates, while the expression of regulatory genes involved in stress response, signaling, and proteolytic degradation is elevated at lower μ. Additionally, transcriptional regulation of many processes related to the secretory pathway, such as protein folding and translocation, is positively correlated with μ [10, 13]. On a metabolic level, fast (but fully respiratory) growth in *S. cerevisiae* has been demonstrated to be accompanied by elevated amino acid pools as well as an increase in glycolytic, pentose-phosphate pathway, and TCA metabolites [11]. The increased productivity at high μ and concordantly rich nutrient conditions agrees well with the respective global rewiring of yeast cells. However, biotechnological production processes (that is, mainly fed-batch cultivation) often need to be operated at lower-than-optimal μ and therefore less-than-optimal productivity. Biomass-specific protein secretion rates of yeasts are usually substantially lower than those achieved by mammalian cell lines [14]. To compensate, yeast-based processes are typically operated at higher cell concentrations, where either mixing, aeration, or cooling capacity ultimately become the limiting aspects for process design

[15, 16]. Furthermore, at higher μ, most of the substrate consumed by the cells is invested in the formation of new biomass, making biomass the most abundant (and typically undesired) by-product. Hence, partial, or ideally, full decoupling of product formation and growth would allow for more efficient production processes and therefore represents an important milestone in the quest for advancing yeast production systems.

In contrast to the vast body of research dedicated to investigating cell physiology and recombinant protein production dynamics at intermediate or higher growth rates, knowledge of the production dynamics of extremely slow or even non-growing yeast remains very scarce. Indeed, extremely slow-growing *S. cerevisiae* cultures have been explored in a non-energy-limited retentostat for the production of succinic acid [17], an important precursor for various chemicals. The non-conventional yeast *Starmerella bombicola*, a natural producer of microbial biosurfactant sophorolipids, was tested for continuous production of bolaform sophorolipid in a similar set-up [18]. However, products like proteins that require a net input of ATP for their synthesis and transport pose a greater challenge [19]. Consequently, microbial production of recombinant proteins at near-zero growth in retentostat cultivation has so far only been attempted in the filamentous fungus *Aspergillus niger* [20].

A well-controlled transition from faster growth rates to theoretically zero growth can be realized via retentostat cultivation, a form of continuous cultivation with full biomass retention. Retentostats are typically initiated from steady-state chemostat cultures. In cases where the energy (and usually also carbon) source is limiting, the respective specific nutrient uptake rate (q_S) asymptotically approaches the specific maintenance energy requirement (m_S), resulting in a scenario where the cells remain in a metabolically active but non-growing state [19]. Aerobic, glucose-limited retentostat cultivation as implemented for *S. cerevisiae*, *Ogataea parapolymorpha*, and *K. phaffii* relies on a gradual decrease of the initial glucose concentration in the feed to a lower setpoint using a mixing vessel upon the switch from the chemostat to the retentostat phase. This setup is specifically beneficial for retentostat cultivation of microbes that exhibit a very low m_S, such as *O. parapolymorpha* and *K. phaffii* [21, 22], for which near-zero growth conditions (μ below 0.001 h^{-1}) can otherwise only be reached after impractically long time periods (described in Vos et al. [23]). Previous retentostat cultivations of *K. phaffii* were only possible when using a *FLO8*-deficient strain, which shows decreased cell adherence to surfaces and is additionally abolished of pseudohyphal growth [21, 24]. Flo8 is a transcriptional master regulator of dimorphism and

cell adherence, and most *S. cerevisiae* laboratory strains are *FLO8*-deficient. In this previous characterization of the non-producing strain at extremely slow growth, it was demonstrated that *K. phaffii* decreases its glucose expenditure on maintenance threefold from 10.0 ± 2.3 to 3.1 ± 0.1 mg g^{-1} h^{-1} with decreasing μ, unlike *S. cerevisiae*, which exhibits a growth rate-independent m_S [21, 23]. Interestingly, growth rate-dependency of m_S was recently also revealed for *O. parapolymorpha* [22].

To test the ability of *K. phaffii* for recombinant protein production and secretion at extremely slow growth, as well as to obtain insights into the physiological adaptations, we conducted aerobic retentostat experiments employing *K. phaffii* CBS2612 *Δflo8* secreting a recombinant antibody protein. Retentostat cultures were analyzed for their growth dynamics, viability, protein secretion capabilities, macromolecular biomass composition, lipidome composition, and transcriptional adaptation patterns. To obtain a more comprehensive picture of the cellular behavior at fast and very slow growth rates, the retentostat data were combined with data from separate chemostat cultivations operated at a dilution rate of 0.1 h^{-1}.

Results

Determination of growth and production parameters of recombinant protein-secreting *K. phaffii*

Choosing a suitable promoter is essential for recombinant protein production at extremely slow growth rates [20]. The ideal candidate should allow for high levels of recombinant gene expression across a wide range of μ and maintain high transcriptional activity in progressing retentostat cultures. Based on microarray transcriptome data from the previous retentostat study using non-producing *K. phaffii* CBS7435 *Δflo8* [21] and the recently discovered beneficial effect of the *Δflo8* mutation on induction strength of the P_{G1}-family in glucose-limiting conditions [25], the P_{G1-3} variant (described as P_{GTH1}-*D1240* in Prielhofer et al. [26]) emerged as the most promising candidate. As a pharmaceutically relevant, stable, and generally well-expressed model protein, a camelid bivalent protein domain antibody (VHH) was chosen [27, 28]. The respective VHH-expressing strain was created previously and assessed in glucose-based small-scale screenings and lab-scale bioreactor-fed-batch cultivations [25].

For accurate growth predictions in retentostat cultures, precise estimates of m_S and the maximum biomass yield (Y_{XS}^{max}) of a specific strain are necessary [23]. While m_S and Y_{XS}^{max} of non-producing *K. phaffii* in glucose-limited retentostat cultures operated at 25 °C were previously determined at 3.1 mg g^{-1} h^{-1} and 0.584 g g^{-1}, respectively, evidence suggests that

recombinant protein production might lead to a higher energy demand for maintenance [10, 29]. Additionally, earlier fed-batch cultivations demonstrated that raising the cultivation temperature from 25 to 30 °C increased the P_{G1-3}-driven production of VHH substantially. As a result, a higher cultivation temperature would likely also result in a higher productivity in the present retentostat study. However, increasing the temperature setpoint adds further uncertainty to the previous estimates of m_S and Y_{XS}^{max}. Hence, m_S and Y_{XS}^{max} were determined for the VHH-producing strain at 30 °C by carrying out eleven separate aerobic glucose-limited chemostat cultivations that were each run at up to two distinct dilution rates (*D*), ranging from 0.015 to 0.17 h^{-1} (Fig. 1A). This simultaneously made it possible to determine the q_P-vs-μ dynamics of P_{G1-3} in the *Δflo8* background. In these chemostat cultures, the highest q_P of 0.64 mg g^{-1} h^{-1} was measured at the fastest *D*-setpoint of 0.17 h^{-1} (Fig. 1A).

Model-based predictions of growth and recombinant protein production in retentostat cultivation

According to the Pirt equation (Eq. 1) [30, 31], the energy-limiting substrate consumed in chemostat cultures (q_S) is distributed over growth, expressed as ($μ/Y_{XS}^{max}$), maintenance (m_S), and, if present, product formation (q_P/Y_{PS}^{max}).

$$q_S = \frac{μ}{Y_{XS}^{max}} + m_S + \frac{q_P}{Y_{PS}^{max}} \tag{1}$$

For organisms that exhibit a growth-independent m_S, this parameter as well as Y_{XS}^{max} can be estimated by plotting q_S against μ. The inverse of the slope will give Y_{XS}^{max}, while the intercept corresponds to the maintenance coefficient [19]. However, for a producing organism, q_P at the respective μ as well as the maximum theoretical product yield (Y_{PS}^{max}) must be known to solve the equation. Y_{PS}^{max} of VHH on glucose was estimated by employing the *K. phaffii* metabolic model [32]. When assuming that glucose is exclusively spent on maintenance as well as recombinant protein synthesis (but not growth), a Y_{PS}^{max} of 0.609 g g^{-1} was predicted. A growth-rate dependency of m_S was observed in the previous retentostat experiment. The non-linear relationship of m_S and Y_{XS}^{max} to μ was identified via sliding-window linear regression analysis on sets of overlapping q_S-vs-μ relations over defined ranges of consecutive μ [21]. A similar analysis of the current data set demonstrated that m_S dropped nearly tenfold between μ of 0.17 and 0.10 h^{-1}, but remained stable at even slower growth rates (Fig. 1B). Similarly, Y_{XS}^{max} dropped by approx. 30%. Interestingly, the decrease in m_S and Y_{XS}^{max} of recombinant protein-producing CBS2612 *Δflo8* at 30 °C seems to take place at a higher μ (above 0.10 h^{-1}) compared to observations of non-producing

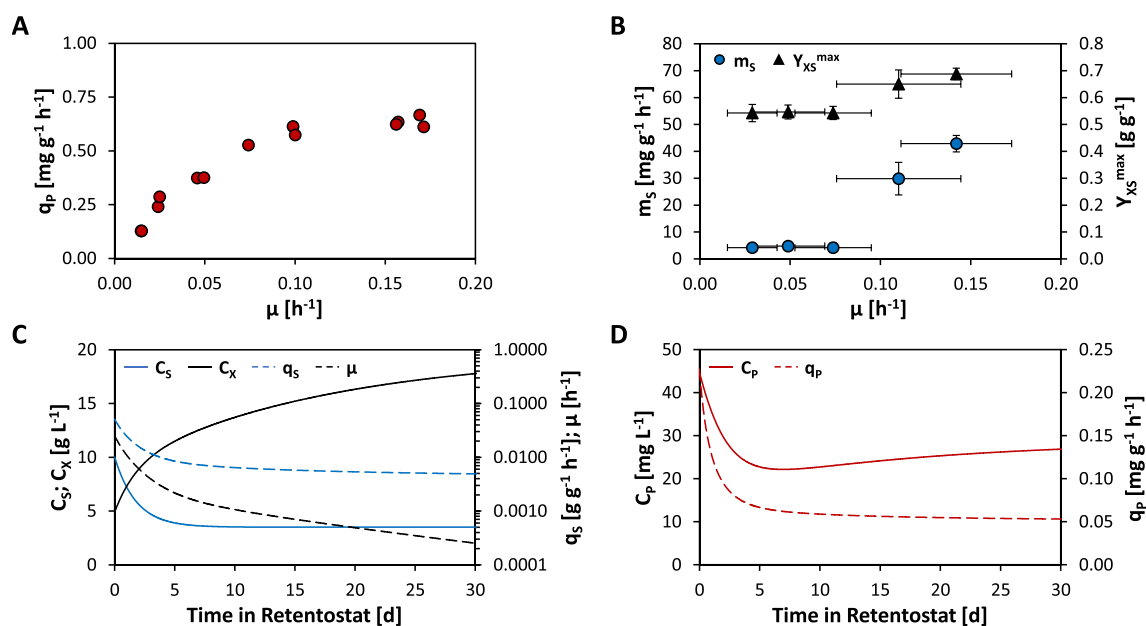Rebnegger *et al. Microbial Cell Factories*   (2024) 23:43

Page 4 of 20

Fig. 1 VHH production and growth parameters estimated from chemostat cultivations and corresponding model-based predictions for retentostat cultures. Aerobic, glucose-limited chemostats for parameter estimation were operated at 7 different dilution rate setpoints ($D = \mu$) ranging from 0.015 to 0.170 h^{-1}. Shown are **A** the biomass-specific VHH secretion rate (q_P) and **B** the maintenance energy requirement (m_S) as well as the maximum theoretical biomass yield (Y_{XS}^{max}) in relation to μ. The dynamics of m_S and Y_{XS}^{max} were estimated by linear regression analysis on moving windows of the specific glucose uptake rate (q_S) as determined from three different consecutive dilution rates and at least two individual cultivations per dilution rate setpoint. **C** Model-based predictions for retentostat cultivations of the biomass built-up (Cx), the glucose concentration in the feed (C_S), μ, q_S, as well as **D** the VHH concentration in the supernatant (C_P) and q_P were calculated based on the average m_S and Y_{XS}^{max} values returned from the three sets of q_S-vs-μ relations for $\mu \leq 0.100$ h^{-1} from (**B**)

CBS7435 *Δflo8* at 25 °C, where substantial changes in m_S and Y_{XS}^{max} were observed down to a μ of 0.05 h^{-1}. Finally, retentostat growth predictions were made using estimates of m_S (4.37 ± 0.27 mg g^{-1} h^{-1}) and Y_{XS}^{max} (0.544 ± 0.002 g g^{-1}), which were calculated by averaging the values returned from linear regression analysis from the three sets of q_S-vs-μ relations of $\mu \leq 0.100$ h^{-1}, where both parameters had stabilized (Fig. 1B). Figure 1C illustrates the predicted profiles of biomass accumulation, μ, and q_S for aerobic glucose-limited retentostat cultures based on an optimized feeding strategy determined by model-aided simulation as described in Rebnegger et al. [21] and Vos et al. [23]. Recombinant protein production was also taken into consideration (Fig. 1D). For simplicity, a linear relationship between μ and q_P was assumed instead of a higher-order function. It was based on linear regression analysis of the q_P-vs-μ relationships of the three lowest μ-setpoints of the chemostat cultivation (Fig. 1A), yielding an intercept of 0.051 mg g^{-1} h^{-1}, theoretically representing q_P at zero growth.

Recombinant protein synthesis and secretion remain active at near-zero growth rates

Retentostat cultivations were initiated from chemostat cultures operated at $D = \mu = 0.025$ h^{-1} and operated for

28 days. Cell viability remained above 90% during the retentostat phase, and the profiles of viable biomass accumulation closely matched those predicted by the model (Fig. 2A). Non-linear regression analysis of biomass accumulation profiles (accounting for recombinant protein production; see Materials and Methods and data presented below as well as Additional file 1: Fig. S1) revealed that on average, the cultures reached a μ of 0.00047 h^{-1} (Fig. 2B), which corresponds to a doubling time of 62 days. The average m_S determined from these cultures was 3.7 ± 0.1 mg g^{-1} h^{-1}, which is almost 20% lower than the estimate obtained from chemostat cultures utilized for model predictions.

Adaptations to near-zero growth rates were dependent on the length of the preceding chemostat phase (Additional file 1: Table S1 and Fig. S2). In fact, retentostat cultures that were in chemostat phase for a longer period of time (18 days; 10.8 volume changes (VC)) had significantly lower viability and biomass yield as well as a nearly two-fold higher maintenance energy requirement than those cultures whose chemostat phase was restricted to 12 days (7.2 VC). As a result, it was decided to limit the time spent in the chemostat phase prior to the initiation of the retentostat phase accordingly. However, while this phenomenon was not explored further in this
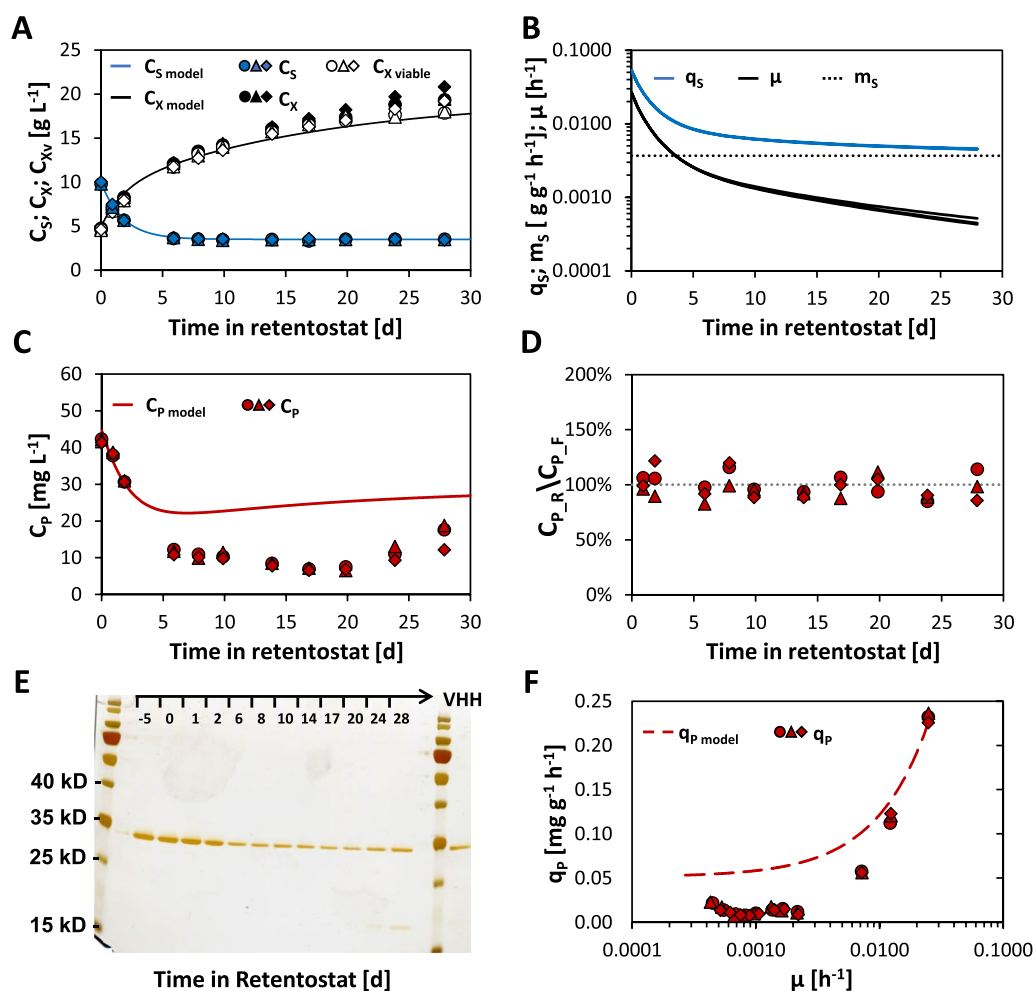
Fig. 2 Aerobic, glucose-limited retentostat cultures of VHH-secreting *K. phaffii*. Retentostat cultures were initiated from chemostat cultures operated at $D = \mu = 0.025$ h^{-1} at time-point zero. Shown are **A** the total (C_X) and viable (C_{Xv}) biomass accumulation profiles and the glucose concentration (C_S) in the feed throughout the retentostat phase as well as corresponding model-based predictions. **B** Estimates of the specific glucose uptake rate (q_S), μ and the average m_S calculated based on non-linear regression analysis. **C** VHH titer (C_P) in supernatants as well as corresponding model predictions based on extrapolation from chemostat data. **D** Ratio of the VHH-titer measured in supernatants (C_{P_R}) and filtrates (C_{P_F}) at the respective sampling point. **E** Representative SDS-PAGE of retentostat supernatants and VHH standard. Protein bands were visualized by silver-staining. **F** Relationship between q_P and μ as well as corresponding model predictions based on extrapolation from chemostat data

study, elucidating the mechanism underlying this behavior might aid in understanding how maintenance is controlled in *K. phaffii* in the future.

This study's main goals included determining if recombinant protein secretion in *K. phaffii* is possible under conditions of almost zero growth. To assess secretion rates and product quality, supernatants and filtrate samples from chemostat and retentostat cultures were analyzed by microfluidic electrophoresis and SDS-PAGE (Fig. 2C–E). Titers were in good agreement with the projected profile during the first two days of retentostat cultivation but remained in the subsequent 8 days approx. twofold and later approx. 3.5-fold below the prediction

(Fig. 2C). Interestingly, product concentrations started to rise again between days 20 and 24, and this trend continued until the end of the retentostat. Product concentrations in the filtrate were comparable to those seen in culture supernatants throughout the whole process (Fig. 2D), indicating that minimal product retention in the bioreactor (if any) takes place. Thus, it can be assumed that the observed VHH levels reflect de novo synthesized and secreted product. Furthermore, despite rising biomass concentrations and slightly declining viability, the concentration of host cell protein in the supernatant remained very low. In agreement, a succinylated-casein-based protease assay showed that protease activity in the

Rebnegger *et al. Microbial Cell Factories*   (2024) 23:43

Page 6 of 20

culture supernatant stayed at background levels until day 20 and slightly increased afterward (Additional file 1: Fig. S3). At the same timepoint, a faint band of approximately 20 kDa occurred (Fig. 2E), which was confirmed by mass spectrometry as a VHH-degradation product (data not shown), suggesting some proteolytic activity at the very end of the retentostat phase.

In the retentostat phase, the measured product titer at a particular time point reflects the biomass concentration, q_P, and initial titers, as well as wash-out dynamics. To estimate q_P in the retentostat phase, a product mass balance was used (see Materials and Methods). Figure 2F shows q_P as a function of μ. In line with expectations, q_P decreased sharply from 0.23 to 0.06 mg g^{-1} h^{-1} over the first two days of retentostat culturing, while μ dropped from 0.025 h^{-1} to 0.008 h^{-1}. At μ below 0.0025 h^{-1}, q_P stabilized, although at roughly fivefold lower levels than those inferred from chemostat data. Consistent with increasing titers, a significant increase in q_P was observed towards the end of the retentostat phase. A drop in P$_{G1-3}$-activity and the resulting lower levels of VHH transcripts during the retentostat phase might explain the significant decline in q_P. P$_{G1-3}$ was chosen as a promoter for VHH expression as *GTH1* was one of the highest expressed genes (according to previous microarray analysis) throughout glucose-limited retentostat cultures of *K. phaffii* CBS7435 *Δflo8* [21]. Stable integration of the VHH expression cassette throughout the retentostat phase was verified by quantitative PCR (qPCR; Additional file 1: Fig. S4), excluding the possibility that the reduced productivity was due to a decrease in the VHH copy number. To assess recombinant gene expression throughout the retentostat phase and compare it to other genes that show natively high expression levels, qPCR employing standards for absolute transcript quantification was conducted. In agreement with the observed q_P profiles (and the obtained RNA-Seq data described below), VHH transcript levels decreased substantially in the early and mid-retentostat phases before returning to chemostat levels at the very end of the retentostat cultivation (Additional file 1: Fig. S5A). *GTH1* expression levels followed a similar pattern but remained at a lower level at the slowest μ. However, absolute *GTH1* levels were slightly higher than those of VHH for most of the investigated sampling points (Additional file 1: Fig. S5B). In the following, VHH transcript levels were also compared to those of *SPI1*, which is one of the strongest, constitutively expressed genes known in *K. phaffii* [33, 34] and ranked among the highest expressed genes in the present RNA-Seq data as well. Indeed, all analyzed samples showed similar or higher VHH levels than those observed for *SPI1*, suggesting that the choice of promoter for retentostat cultivations was indeed appropriate.

K. phaffii changes its biomass composition when approaching near-zero growth rates

Biomass composition has been demonstrated to change with growth rate as well as the respective (limiting) nutrient source in chemostat and retentostat cultures [32, 35–37]. Hence, to investigate to what degree and in what manner the biomass composition changes when recombinant *K. phaffii* approaches near-zero growth rates, samples from separate chemostats operated at $D = μ = 0.10$ h^{-1}, cultures in chemostat phase ($D = μ = 0.025$ h^{-1}; day 0) and retentostat phase from days 14 and 28 (corresponding to μ of 0.0010 and 0.00047 h^{-1}, respectively) were analyzed for their total carbohydrate, protein, RNA, DNA, and lipid content, as well as their amino acid, lipid class, and elemental composition (Fig. 3A, Additional file 1: Tables S2 and S3 as well as Additional file 2). Additionally, a subset of the analyses was also done on retentostat samples taken on day 6 (corresponding to a μ of 0.0022 h^{-1}).

Across all growth rates, the largest fraction of biomass was composed of carbohydrates, followed by protein and RNA. In agreement with previous reports of *K. phaffii* X-33 and *S. cerevisiae* grown on glucose, a negative relationship between μ and the total carbohydrate content was observed [32, 35]. However, in the present study, significant changes (p-value < 0.05; Additional file 1: Table S4) were only seen between μ of 0.10 and 0.025 h^{-1}, while the total carbohydrate content remained rather stable at 54–55% throughout the retentostat phase. Down to a μ of 0.0022 h^{-1}, the increase in total carbohydrate content was accompanied by steadily increasing levels of the storage carbohydrate trehalose, which reached a maximum of 14.7% (w/w) at day 6 of retentostat cultivation but started to decrease again thereafter (Fig. 3B). On the other hand, levels of the second main storage carbohydrate, glycogen, remained relatively stable at approx. 5% down to a μ of 0.0014 h^{-1}, before decreasing to 2.9% throughout the remaining retentostat phase. Hence, storage carbohydrate metabolism appeared to be regulated similarly in recombinant protein-secreting CBS2612 *Δflo8* as compared to non-producing CBS7435 *Δflo8* [21]. Interestingly, the amount of other carbohydrates also decreased with decreasing μ to 33.3% (w/w) on day 6 before increasing again to 39.2% at the end of the retentostat culture (Fig. 3B).

The amount of total RNA and DNA decreased with decreasing μ (Fig. 3A and Additional file 1: Table S2). The RNA content dropped from 4.6 to 3.8% between μ of 0.10 and 0.025 h^{-1} and reached 3.4% at the end of the retentostat phase, while the total DNA content dropped the most in the early retentostat phase from 0.7 to 0.4%. The total protein content also showed a clear correlation with growth between μ of 0.1 and 0.0022 h^{-1},
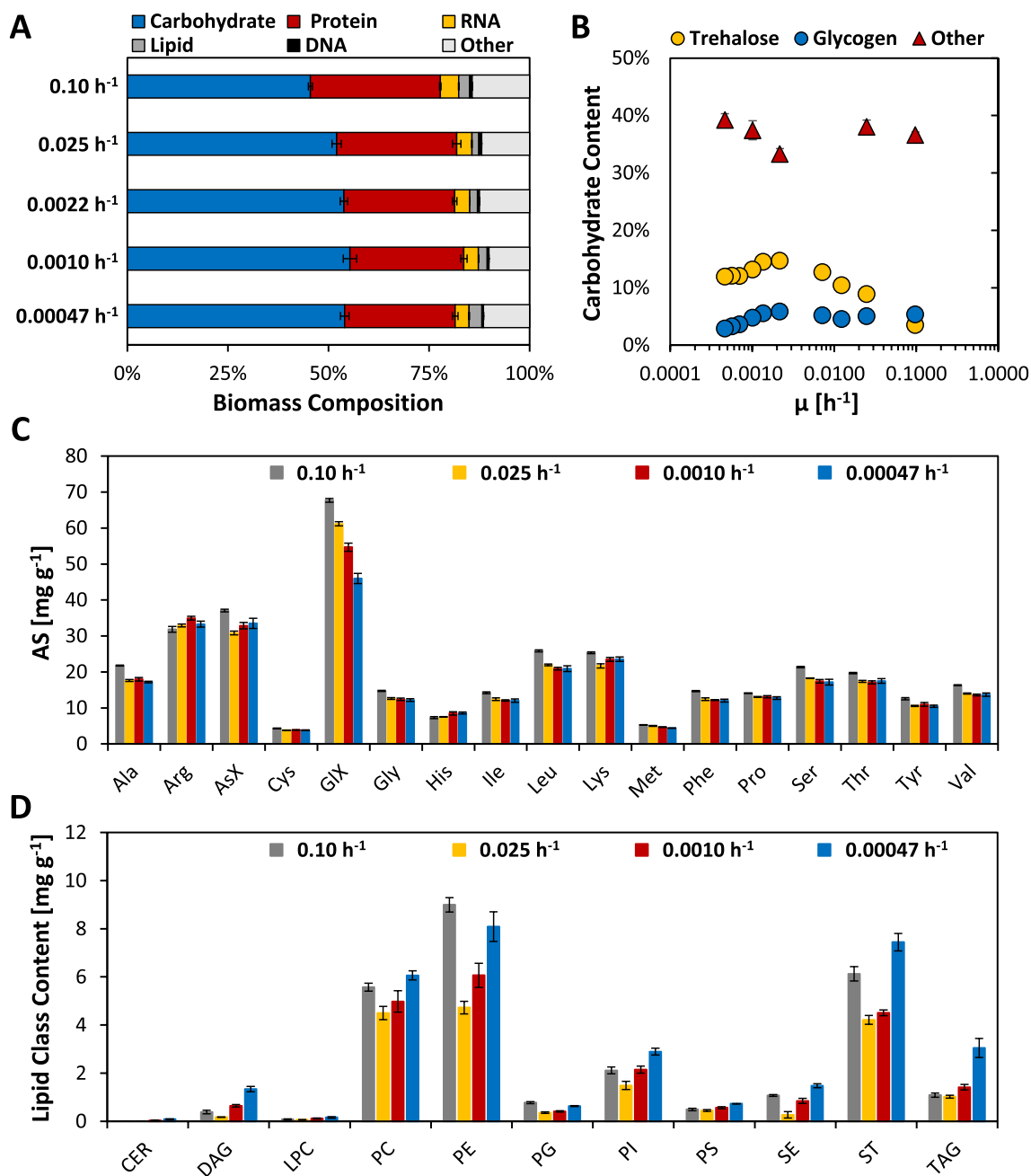
Fig. 3 Biomass composition of recombinant *K. phaffii* over a wide range of μ. Samples were taken from separate chemostat cultures operated at $D=\mu=0.1$ h^{-1}, retentostat cultures in the chemostat phase ($D=\mu=0.025$ h^{-1}; day 0), and throughout the retentostat phase ($\mu < 0.025$ h^{-1}). **A** Macromolecular biomass composition; and **B** percentage of storage carbohydrate content and other carbohydrates. **C** Amino acid content measured in hydrolysates of whole cells. GlX represents the sum of Glu and Gln and AsX the sum of Asp and Asn. Tyrosine was not measured. **D** Lipid class content, including ceramide (CER), diacylglycerol (DAG), lyso-phosphatidylcholine (LPC), phosphatidylcholine (PC), phosphatidylethanolamine (PE), phosphatidylglycerol (PG), phosphatidylinositol (PI), phosphatidylserine (PS), sterol ester (SE), sterol (ST), triacylglycerol (TAG). All biomass composition data for the main sampling points is also provided in Additional file 2

where it dropped from 32.3 to 27.5%, while it remained relatively stable from the mid-retentostat phase on when cells approached near-zero growth conditions. This pattern was well reflected by the elemental nitrogen content

(Additional file 1: Table S3) as well as the amino acid levels, which represented the amino acid content of whole cell hydrolysates (free amino acids are neglectable) (Fig. 3C). Pronounced changes in terms of amino

Rebnegger *et al. Microbial Cell Factories*   (2024) 23:43

Page 8 of 20

acid level were observed for GlX (referring to the sum of glutamine and glutamic acid), which decreased by approximately 30%. For *S. cerevisiae*, free glutamine has been proposed as a "signature metabolite" that indicates carbon source abundance [11], while glutamic acid pools showed a more diverse pattern. Both free metabolites show a high abundance in comparison to the majority of other free amino acids. It would be tempting to speculate that assumedly low pools of free glutamine at severe calorie restriction might also be reflected in the whole cell hydrolysate glutamine content. Unfortunately, with the method employed in this study, it was impossible to distinguish between glutamine and glutamatic acid.

Lipidomics reveals an increase in neutral lipid content toward zero growth

The total lipid content and composition of yeasts can be considerably impacted by changes in growth conditions, such as different growth phases, carbon sources, or oxygen availability [38–41]. For *K. phaffii,* significant differences between glucose and methanol conditions were seen regarding triacylglycerol (TAG) content, while over the course of a glycerol batch-phase and a methanol feed-phase, major changes in various phospholipid levels were observed [39, 41]. However, adaptations of the cellular lipidome in relation to growth rate and/or severe calorie restriction have not been investigated so far. Lipidome analysis was done by employing reversed phase liquid chromatography (RP-LC) coupled to high-resolution mass spectrometry (HRMS). Detailed information on the respective lipid class levels as well as the respective species composition is provided in Additional file 2. Overall, the total lipid content showed a more complex pattern compared to other macromolecules, as levels decreased from 2.7 to 1.7% between μ of 0.10 and 0.025 h^{-1}, and rose again to 3.2% over the course of the retentostat cultivation. While nearly all individual lipid classes showed a similar trend, phosphatidylethanolamines (PE), sterols (ST), and TAG contributed the most to the total increase in lipid content at the end of the retentostat phase (Fig. 3D). The main sterol in fungi and yeast is ergosterol, which is also the major lipid regulating membrane fluidity and other important biological processes such as endocytosis, cytoskeleton organization, and mating [42, 43]. Furthermore, it is suspected that ST content (and therefore membrane properties) affects recombinant protein secretion [40, 44]. TAG, as well as sterol esters (SE), are neutral lipids that can form lipid droplets (LD), which are very dynamic organelles that are involved in energy and lipid homeostasis, as well as several other biological processes [45, 46]. The size of LDs is reported to increase in late log- and early stationary-phase cultures [47]. SE content in this study followed the general lipid trend, with levels strongly decreasing between μ of 0.10 h^{-1} and 0.025 h^{-1}, and gradually increasing again in the retentostat phase. TAG, which has been identified as the primary component of LDs in *K. phaffii* [48], remains at similar levels in the investigated chemostat cultures and up to the mid-retentostat phase, while its levels more than double at the end of the retentostat cultivation. Accordingly, levels of diacylglycerol (DAG), which functions as a precursor for TAG synthesis in the context of LD formation [49], increase nearly eightfold throughout the retentostat phase. Staining of cells with the lipophilic dye Nile red (NR) and subsequent analysis by cytometry and fluorescence microscopy revealed that the fraction of NR-positive cells decreases substantially with decreasing μ (Additional file 1: Fig. S6A), with the exception of the sample taken at the end of the retentostat, for which an increase in NR-staining was observed. However, while the fraction of NR-positive cells in the retentostat phase was much lower, their fluorescence intensity increased more than fivefold (Additional file 1: Fig. S6A). Fluorescence microscopy confirmed these patterns (Additional file 1: Fig. S6B). Remarkably, staining patterns in faster-growing cells were more diffuse, rarely showing a clear LD pattern, while in the retentostat phase, NR-positive cells mostly showed the characteristic LD pattern.

Global transcriptional regulation patterns of recombinant *K. phaffii* at extremely low growth reveal that growth rate rather than protein production is the major determinant

Global transcriptional adaptation of VHH-secreting CBS2612 *Δflo8* towards near-zero growth rates was investigated by RNA-Seq. Samples for RNA-Seq analysis were taken from separate chemostats operated at D=μ=0.10 h^{-1}, retentostat cultures operated in chemostat mode just before entering the retentostat phase ($D=$μ=0.025 h^{-1}; day 0) and retentostat samples from days 6, 14, and 28, corresponding to specific μ of 0.0022 h^{-1}, 0.0010 h^{-1}, and of 0.00047 h^{-1}, respectively. Out of 5343 ORFs annotated as protein-encoding genes, 1405 were differentially expressed (FC≥2; adj. *p*-value≤0.01) in at least one comparison against the 0.1 h^{-1} setpoint. *k*-means cluster analysis revealed four primary regulatory patterns (Fig. 4A), with genes displaying either moderate or strong up- or down-regulation toward zero growth. Detailed information on the clusters and corresponding enriched GO terms are provided in Additional file 2. A large majority of the differentially expressed genes (approximately 80%) displayed a rather moderate regulation trend, whereas the distribution between up- (48%) and down-regulated (52%) genes was fairly even.

Significantly enriched GO terms among moderately and strongly downregulated genes towards zero growth

Rebnegger *et al. Microbial Cell Factories*   (2024) 23:43

Page 9 of 20

(Cluster 1 and 2, respectively) largely overlapped and were almost exclusively related to the (mitotic) cell cycle and respective cell-cycle associated processes, which were also down-regulated with μ in the previous retentostat study using non-producing CBS7435 *Δflo8* [21]. Genes associated with the "cell wall" were also enriched in both clusters, including the major *K. phaffii* cell wall genes *TIP1, PIR1, PIR2,* and *BGL2.* Furthermore, nearly all histone-encoding genes were strongly downregulated with decreasing μ and therefore clustered into Cluster 2. Expression of histones has been demonstrated to be regulated in a cell-cycle-dependent manner in *S. cerevisiae* before [50], and strong downregulation of histone genes was observed in previous retentostat cultivations as well [21]. Even though transcriptional downregulation of genes involved in protein biosynthesis is commonly observed in yeast and bacteria in response to slow growth conditions [19], no GO terms related to protein biosynthesis were enriched in Clusters 1 and 2. Examining the genes that encode the 60S and 40S ribosomal subunit proteins in more detail revealed that, in fact, only 22 of the 87 known genes were significantly downregulated in at least one comparison and that the majority of the corresponding transcript levels only exhibited a negative correlation trend towards zero growth. On the other hand, total RNA levels showed a slight but significant drop between μ of 0.10 and 0.025 h^{-1}, where only a single ribosomal gene was differentially expressed, indicating that total RNA content and ribosomal gene expression are not strictly correlated in *K. phaffii* under the investigated growth conditions. Mitochondrial translation appears to be even less affected by slow growth, as only one out of 76 genes encoding subunits of the mitochondrial ribosome was significantly downregulated.

In the previous retentostat study of the non-producing *K. phaffii* strain, ergosterol biosynthesis genes were overrepresented among those downregulated towards near-zero growth rates [21]. Despite this not being the case in the current GO analysis, 11 out of 26 genes with a central role in the ergosterol pathway had significantly reduced expression levels in retentostat cultures, and 7 additional genes had a similar regulation trend. Total ST content significantly decreased between μ of 0.1 h^{-1} and 0.025 h^{-1} from 6.1 to 4.2 mg g^{-1}, remaining at this level throughout the early retentostat phase, and significantly increased again during the late retentostat phase to 7.4 mg g^{-1}. Interestingly, and somewhat in contrast to the lipid content measurements, substantial downregulation of the ergosterol pathway genes was only observed in the sample taken in the early retentostat phase (day 6; μ = 0.0022 h^{-1}), but not at the 0.025 h^{-1} setpoint. Furthermore, although ergosterol content at the end of the retentostat phase exceeded those levels measured at the 0.1 h^{-1} setpoint, the expression of most genes remained at those levels observed in the mid-retentostat phase. The transcript levels of *ARE2*, the primary gene responsible for sterol esterification in *K. phaffii* [51], were markedly increased in the early and mid-retentostat phases, which is consistent with rising SE levels in progressing retentostats. The expression profiles of the respective genes involved in TAG biosynthesis, however, did not match its measured content. *LRO1*, the major gene responsible for TAG synthesis in *K. phaffii* [51], was significantly downregulated throughout the retentostat phase, while TAG content remained relatively stable until the second half of the retentostat phase, during which it increased by more than twofold (Fig. 3D). *DGA1*, on the other hand, showed a strong positive regulation trend with a declining growth rate despite being predicted to have a reduced function in TAG synthesis in this yeast under conventional growth conditions. Furthermore, whereas *K. phaffii's* overall PE content varied significantly, neither the expression levels of the two phosphatidylserine decarboxylases, which synthesize PE from phosphatidylserine (PS) (*PSD1* and *PSD2*; [52]), nor the levels of the genes that synthesize PE from ethanolamine (*CKI1, ECT1,* and *EPT1*) were differentially regulated. In conclusion, the observed changes in lipid class content correlated only poorly with the transcriptional patterns of the genes involved in their production. In Additional file 2, a comprehensive list of lipid biosynthetic genes and the respective differential gene expression data is included.

Only a few enriched GO terms were identified in the two gene sets upregulated towards zero growth.

(See figure on next page.)

Fig. 4 *k*-means cluster analysis, corresponding enriched GO terms, and regulatory trends of secretory pathway genes. **A** Samples for RNA-Seq analysis were taken from separate chemostat cultures operated at $D = μ = 0.1 \, h^{-1}$, retentostat cultures in the chemostat phase ($D = μ = 0.025 \, h^{-1}$; day 0), and throughout the retentostat phase (μ < 0.025 h^{-1}; days 6, 14 and 28). Genes that were differentially expressed compared to the highest μ of 0.10 h^{-1} (FC ≥ 2; adj. *p*-value ≤ 0.01) in at least one comparison were grouped into four clusters by *k*-means clustering and analyzed for enriched GO terms. A comprehensive list of all enriched GO terms of the categories biological process (BP), molecular function (MF), and cellular component (CC) identified in the analysis is provided in Additional file 2. Enriched GO terms for Clusters 1 and 2 overlapped to a high degree. The main terms shared between these two clusters as well as all enriched GO terms from Clusters 3 and 4 were listed, respectively. **B** Total numbers of genes allocated to biological processes related to the secretory pathway and relative numbers of regulated genes. Color intensities reflect the degree of regulation of the respective group
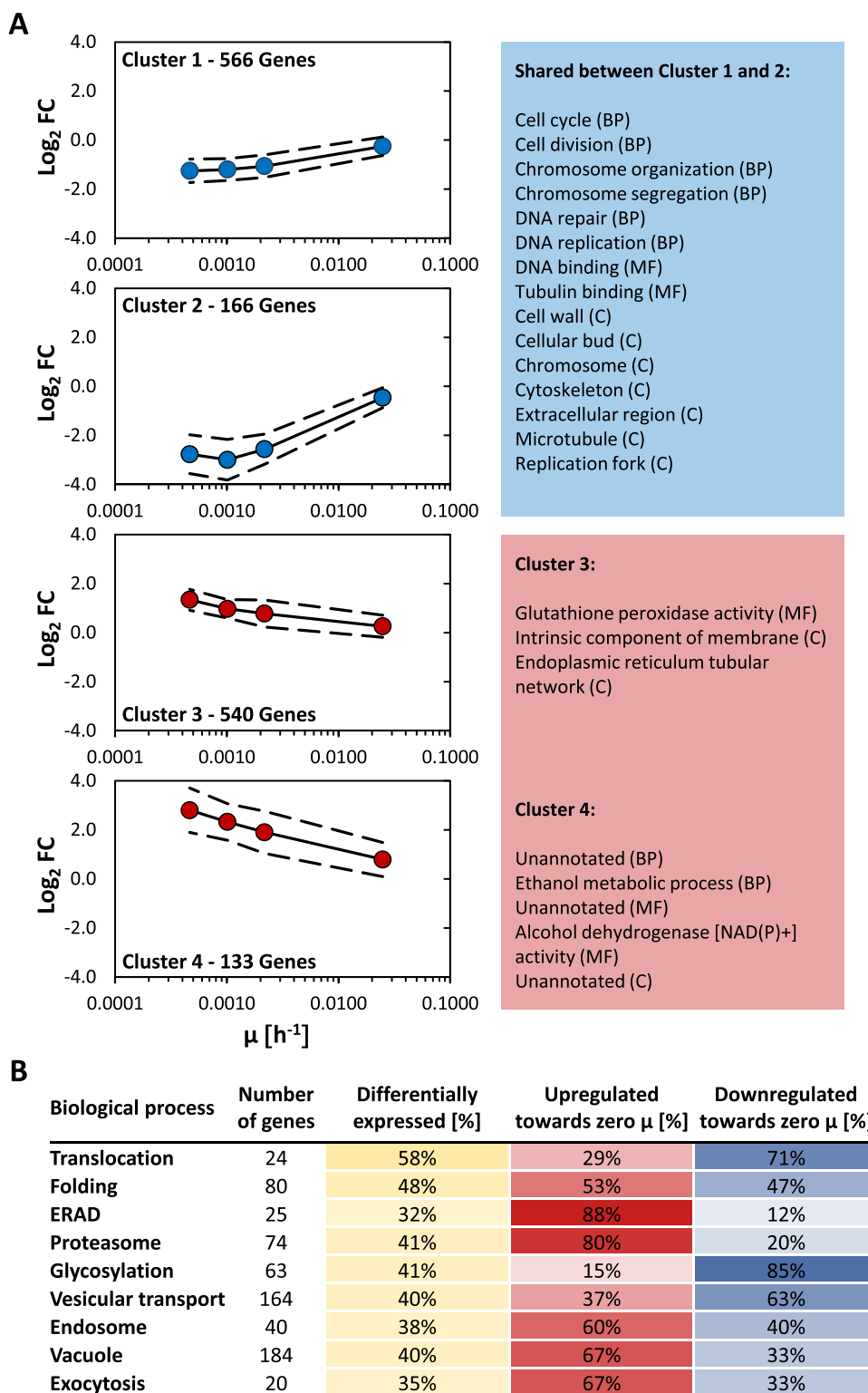
A

Cluster 1 - 566 Genes

Cluster 2 - 166 Genes

Cluster 3 - 540 Genes

Cluster 4 - 133 Genes

Shared between Cluster 1 and 2:

Cell cycle (BP)
Cell division (BP)
Chromosome organization (BP)
Chromosome segregation (BP)
DNA repair (BP)
DNA replication (BP)
DNA binding (MF)
Tubulin binding (MF)
Cell wall (C)
Cellular bud (C)
Chromosome (C)
Cytoskeleton (C)
Extracellular region (C)
Microtubule (C)
Replication fork (C)

Cluster 3:

Glutathione peroxidase activity (MF)
Intrinsic component of membrane (C)
Endoplasmic reticulum tubular
network (C)

Cluster 4:

Unannotated (BP)
Ethanol metabolic process (BP)
Unannotated (MF)
Alcohol dehydrogenase [NAD(P)+]
activity (MF)
Unannotated (C)

B

Biological process	Number of genes	Differentially expressed [%]	Upregulated towards zero μ [%]	Downregulated towards zero μ [%]
Translocation	24	58%	29%	71%
Folding	80	48%	53%	47%
ERAD	25	32%	88%	12%
Proteasome	74	41%	80%	20%
Glycosylation	63	41%	15%	85%
Vesicular transport	164	40%	37%	63%
Endosome	40	38%	60%	40%
Vacuole	184	40%	67%	33%
Exocytosis	20	35%	67%	33%

Fig. 4 (See legend on previous page.)

Overrepresented genes that were grouped into Cluster 3 (moderate upregulation) were involved in "glutathione peroxidase activity", "intrinsic component of membrane" and "endoplasmic reticulum tubular network". In Cluster 4 (strong upregulation towards zero growth), "unannotated" genes as well as genes with alcohol or aldehyde dehydrogenase activity were found to be overrepresented.

However, while only a limited number of GO terms were found to be enriched, many of the genes that were grouped into clusters 3 and 4 showed the same trend in regulation in the previous retentostat study. For example, genes encoding main stress response transcriptional regulators such as *HAC1*, *MSN4*, *SKO1*, and *YAP1*, respective (oxidative) stress-responsive genes (e.g., *SOD1*, *MXR1-2*, *MXR2-1*, *MXR2-2*, *GRX2*, *HSP31*, *HSP60*), as well as genes involved in transcriptional regulation of nutrient response (e.g. *CAT8-2*, *MIT1*, *GAT1*, and *NRG1*) grouped into clusters 3 and 4. In agreement, many genes with a role in nitrogen catabolite repression (NCR) and alternative carbon source utilization were upregulated as well, including *GAT1* (a main transcriptional activator of NCR) and the main methanol (*AOX1*, *AOX2*, *DAS1*, and *DAS2*) and ethanol (*ADH2*, *ADH600*, and *ADH900*) utilization genes. As described previously, upregulation of NCR genes is not only restricted to low nitrogen conditions but was also observed upon glucose limitation in *S. cerevisiae* [53], and de-repression of methanol and ethanol utilization genes caused by very low glucose levels likely primes the cells to readily metabolize any suitable alternative carbon source if it suddenly becomes available. This behavior represents a "be-prepared" survival strategy and is a common reaction in response to severe calorie restriction in filamentous fungi, yeast, and bacteria [19, 54].

Transcriptional regulation of secretory pathway genes at near-zero growth rates

Based on the focus of this work on recombinant protein secretion dynamics at extremely slow growth rates, a more in-depth analysis was applied to genes with a function in the secretory pathway, including protein translocation into the endoplasmic reticulum (ER), folding, N- and O-glycosylation, ER-associated protein degradation (ERAD), proteasomal genes and genes of the ubiquitin–proteasome system, vesicular transport, endosome, vacuole, as well as exocytosis. For this analysis, a lower fold-change threshold (1.5 instead of 2) was used to determine whether genes were differentially expressed. Figure 4B provides a summary of the regulatory patterns for the key mechanisms involved in protein secretion. The expression of those genes with a role in co- or posttranslational translocation of the nascent aminopeptide chain into the ER was affected the most by variations in μ. In this cohort, the majority of significantly regulated genes had their expression downregulated, approaching zero growth. Similar findings were made previously for HSA-secreting *K. phaffii* SMD1168H cultivated in glucose-limited chemostat cultures at faster growth rates ranging between 0.015 and 0.15 h^{-1} [10]. Expression of genes involved in protein folding was also strongly affected. However, unlike at faster μ, where a clear positive correlation with the growth rate was observed, the distribution between up- and downregulated genes at extremely slow growth was nearly even. In this regard, it is interesting to note that the expression of *HAC1* (main transcriptional regulator of the unfolded protein response; UPR) was significantly upregulated from mid-retentostat phase on, while it showed a positive correlation with growth in the previous study. However, known UPR targets of *HAC1* were found in both groups, including genes with markedly increased (*KAR2*, *ERO1*, *HSP82*) or decreased (*SCJ1*, *SSA1*, *MPD1*) transcript levels at near-zero growth rates. About 41% of genes with a known function related to core oligosaccharide synthesis, or N- or O-glycosylation, were differentially expressed, and 85% of them were found to be downregulated towards near-zero growth. A positive regulation trend with growth was also observed at faster μ, albeit to a lesser extent. Transcript levels of genes with a function in ERAD as well as the ubiquitin–proteasome system and proteasome-subunit-encoding genes were less affected. However, of those genes that were differentially expressed, 88% of ERAD− as well as 80% of proteasome-related genes were upregulated throughout the retentostat phase. The majority of significantly regulated genes related to the endosome and vacuole showed higher expression levels at extremely slow growth as well, and all genes with a primary function in autophagy displayed a similar trend, further demonstrating that activation of proteolysis is a main response at near-zero growth rates.

Interestingly, while a majority of differentially expressed SNAREs and other genes involved in vesicular transport were downregulated at slow growth, genes involved in exocytosis were mostly upregulated. Taken together, the data shows that numerous processes that drive protein maturation and secretion are impacted at near-zero growth rates and that their regulatory patterns can diverge from those seen in chemostats at faster μ. However, the data also clearly demonstrate that many processes at extremely slow growth are regulated in a manner that seems predominantly detrimental to protein secretion.

Rebnegger *et al. Microbial Cell Factories* (2024) 23:43

Page 12 of 20

Discussion

In this study, the recombinant protein production kinetics of *K. phaffii* CBS2612 *Δflo8* were examined over a broad range of μ in aerobic, glucose-limited chemostat and retentostat cultures. In the latter, doubling times of approximately 2 months were reached, corresponding to a μ of 0.00047 h^{-1}. One of the main goals was to determine whether and, if so, to what extent recombinant protein secretion is sustained at such extremely low growth rates. Maximum specific VHH secretion rates driven by the glucose-limit-induced promoter P$_{G1-3}$ in the *Δflo8* background were observed at the fastest investigated $D = μ$ of 0.17 h^{-1}. De novo synthesis and secretion of VHH were indeed maintained throughout retentostat cultivation, but the lowest q$_P$ was roughly fivefold lower than what was anticipated from chemostat cultivations. Recombinant gene transcript levels significantly decreased along with decreasing secretion levels in the retentostat phase, but to a considerably lesser extent than what was shown in terms of q$_P$. However, it should be noted that rising VHH transcript levels did, in fact, correspond to rising productivity at the end of the retentostat phase, demonstrating that transcriptional regulation of the recombinant gene might be partially responsible for the diminished production capacity of the cells, but other factors clearly play a role as well.

Translation is one of the key steps involved in recombinant protein production, and it has been shown in several studies that *S. cerevisiae* and bacteria downregulate the energetically costly translational machinery in progressing retentostat cultures [19, 23]. In contrast, in *K. phaffii*, we did not observe enrichment of GO terms related to protein biosynthesis in the significantly down-regulated gene set, neither in the previous retentostat study [21] nor in this study, although many of the respective genes showed a negative regulation trend. Total RNA (which is to a large degree comprised of ribosomal RNA) as well as total protein levels did indeed drop slightly when cells approached zero growth. However, q$_P$ decreased much more rapidly than it would be anticipated from the regulation trends of the translational machinery genes and macromolecular biomass composition data.

Multiple studies have concluded that protein folding and maturation are the main bottlenecks in the production process of secretory recombinant proteins. Consequently, many factors that are involved in protein secretion have been targeted in cell engineering approaches, albeit with varying success (reviewed e.g. by Madhavan et al. [55], Raschmanová et al. [56], and Zahrl et al. [57]). The importance of certain steps of the secretion pathway, such as folding and disulfide bond formation, has previously been established. Furthermore, it was demonstrated for *K. phaffii* and *S. cerevisiae* that

increased secretion capacities correlate strongly with the increased expression of genes involved in these key processes, such as translocation, glycosylation, and folding. In contrast, proteolytic processes such as ERAD or vacuolar genes show much lower expression levels at fast μ [10, 13]. In the current study, it was demonstrated that the regulation of secretory pathway genes at near-zero growth deviates from trends observed at faster μ. For example, *HAC1*, the main transcriptional activator of UPR in *K. phaffii*, as well as several of its main target genes, are upregulated towards zero growth, while its expression showed a positive correlation to μ in faster-growing chemostat cultures. *HAC1* overexpression has been demonstrated to increase secreted recombinant protein levels in the past [56], and its upregulation together with some of its targets might benefit protein secretion. However, we observed a simultaneous strong upregulation of genes involved in proteolytic processes, including proteasomal and ERAD genes, as well as vacuolar genes and genes related to autophagy. Furthermore, key genes involved in protein translocation into the ER were strongly downregulated, resulting in a regulatory pattern of secretory pathway genes that seems mostly detrimental to efficient protein secretion.

The choice of a suitable promoter has previously been identified as a key factor in successful recombinant protein secretion at near-zero growth rates, with very little secreted product detected from malate-limited retentostat cultivations of the filamentous fungus *A. niger* [20]. However, the two tested *A. niger* promoters were mainly active at μ > 0.001 h^{-1}, while P$_{G1-3}$ in this study allowed for high expression of the VHH across the entirety of investigated growth rates.

Full decoupling of growth and recombinant protein production in *K. phaffii* has been realized in a strain lacking the genes for alcohol oxidase, which represent the first step of methanol utilization, and methanol-based induction of the *AOX1* promoter [58]. Specific secretion rates of the same model protein as employed in the present study throughout the methanol-production phase were on average 0.088 mg g^{-1} h^{-1}, and therefore ca. fivefold higher than the q$_P$ observed at the end of the retentostat cultivation. MeOH uptake rates were 1.6-fold higher than the reported m$_S$ on methanol, while in this study glucose uptake at day 28 exceeded the estimated m$_S$ by 25%. Furthermore, the actual non-growth production phase in the methanol-based approach only lasted 72 h, and it is unclear for how long the cells would sustain the observed level of productivity. A possible explanation for higher secretion rates in methanol conditions would be that growth on this carbon source is natively accompanied by very high expression of methanol utilization genes such as Aox1 [59], and methanol-grown

cultures might therefore generally sustain high translation activity. However, in a recent study, translation activity at intermediate growth rates was comparable between methanol and glucose-limited conditions [60]. Another explanation would be that expression of the recombinant gene remained higher in the P_{AOX1}-based system, which, however, would be very difficult to compare directly.

The current study provides a comprehensive analysis of how the macromolecular biomass composition of recombinant *K. phaffii* changes when cells transition to near-zero growth conditions. In essence, the observed regulation trends of the total protein, RNA, and carbohydrate content are similar to what has been observed at faster µ, namely a decrease in total RNA, DNA, and protein content while the total carbohydrate content increases with decreasing µ [32]. In contrast to the total protein, RNA, and carbohydrate content, the DNA content changed the most in the retentostat phase. Lipid content and composition, on the other hand, showed a more complex trend in their regulation. Information on how the macromolecular biomass composition changes when yeast cells approach near-zero growth has so far only been obtained to a limited extent in non-energy-limited *S. cerevisiae* retentostat cultures. In these conditions, Liu et al. [37] reported a significant change in the total protein content for both nitrogen- and phosphor-limited cultures when µ was decreased from 0.025 h^{-1} to below 0.002 h^{-1}. Total carbohydrate, RNA, DNA, or lipid content were not investigated, but total carbon content increased in both conditions. Interestingly, changes in total protein content in N- and P-limited cultures of *S. cerevisiae* were much larger compared to what was observed for *K. phaffii* in this study.

Coltman et al. [67] used the here presented cultivation and biomass composition data to investigate the metabolic rewiring of *K. phaffii* in response to extremely slow growth rates by flux balance analysis and flux sampling. According to this study, *K. phaffii* mainly adapted to severe calorie restriction by reducing flux through the pentose phosphate pathway, and channeling a greater proportion though glycolysis and the TCA cycle. This contributed, among others, to a higher yield of ATP per consumed glucose.

The amino acid composition of the whole cell lysate changed only slightly with µ. Large changes were only detected for the sum parameter of glutamic acid and glutamine. When comparing the fast µ set-point in this study to the respective amino acid distribution described by Carnicer et al. [61] for 21% oxygen, most values are within good agreement (< 16% relative change, Additional file 1: Table S5). Cysteine and methionine, however, were not protected via oxidation prior to HCl hydrolysis in the previous study, resulting in their underestimation [62].

Consequently, values for methionine were 1.6-fold higher and for cysteine even more than eightfold higher in our study when compared to the highest levels reported for *K. phaffii* by Carnicer et al. [61]. In contrast to Carnicer et al. [61] we do not report any values for tryptophan as it is known to fully degrade during HCl hydrolysis and could also not be detected after MSA hydrolysis. We obtained 15 to 16% higher values for AsX, proline, serine, and tyrosine, all of which were measured after MSA hydrolysis. Serine, tyrosine and threonine are known to be partially degraded during HCl hydrolysis [63], which was the only hydrolysis method employed by Carnicer et al. [61]. On the other hand, we observed 5 to 16% lower values for valine, GlX, alanine, isoleucine, histidine, and arginine. This finding can only in part be explained by the fact that the values being compared here are percentages. Besides the application of two independent acidic hydrolysis methods, another major difference in methodology employed in comparison to previous studies analyzing *K. phaffii* protein amino acid composition on glucose and other carbon sources [32, 61, 64], is the fact that our analytical workflow made use of MS detection. Hence, we could base quantification on external calibration and internal standardization with heavy isotope-labeled (i.e., chemically identical) internal standards. These internal standards were added prior to hydrolysis to improve the accuracy of sample preparation and analysis, including this first sample preparation step. Consequently, the method employed in this study should reflect the actual amino acid composition of hydrolyzed *K. phaffii* whole cells more accurately than the previous measurements employing only HCL hydrolysis [32, 61, 64] and therefore represents a valuable contribution to the biomass characterization of *K. phaffii* in general. It has to be mentioned, however, that isoleucine, valine and leucine might be also underestimated in our study as hydrolysis is not 100% efficient for certain amino acid sequences [62, 63].

Changes in total lipid content as well as lipid class and species composition were analyzed by RP-LC-HRMS. Interestingly, the overall lipid content was approximately 40% lower in cells cultivated at a µ of 0.025 h^{-1} compared to those grown at 0.1 h^{-1} in chemostat cultures, but the trend fully reversed throughout retentostat cultivation. At the very end of the retentostat phase, total lipid levels even exceeded those measured from the 0.1 h^{-1} chemostat samples. This increase was to a large degree based on the rise in PE, ST, and TAG levels. PE and the main sterol in yeast, ergosterol, are polar and major components of cellular membranes, while TAG is a neutral lipid and the main component of lipid droplets in *K. phaffii* [48, 65, 66]. While a wide array of functions are attributed to lipid droplets, their core and potentially most ancient function is to serve

as a nutrient reservoir [49]. Accordingly, lipid droplet formation in *S. cerevisiae* is reported to accelerate in the late exponential phase when cells enter the diauxic shift and nutrients become increasingly limiting [47, 49]. Also, in *K. phaffii*, LD formation is increased in late exponential and early stationary phase [48]. In this regard, it is somewhat curious that we see the lowest levels of TAG and sterol ester, the second major neutral lipid present in lipid droplets, in the 0.025 h^{-1} chemostat samples. In fact, lipid droplets were mostly observed later in the retentostat phase. Hence, lipid droplet formation might be regulated differently in cells that are slowly transitioning to near-zero growth conditions, in contrast to those cells that find themselves in much more rapidly depleting nutrient conditions at the end of batch culture.

Conclusions

This study demonstrates that the production of recombinant secretory proteins by *K. phaffii* is feasible in near-zero growth conditions in glucose-limited retentostat cultures, although titers and production rates remained lower than predicted based on extrapolations from faster μ investigated in chemostat cultures. The comprehensive macromolecular and omics data set pinpoints potential cell engineering targets, such as the translocation process that has recently been identified as rate-limiting [68]. Changes in lipid metabolism reveal a complex adaptation pattern towards very slow growth rates. The higher abundance of storage lipids as well as storage carbohydrates indicates that the cells are preparing for long-term survival. On the other hand, the restored abundance of membrane-forming lipid classes such as PE, PC, and sterols towards zero growth might contribute to the still active secretory pathway under these scarce conditions.

Materials and methods
Strains and culture conditions

As a base strain, *K. phaffii* CBS2612 (CBS-KNAW Fungal Biodiversity Centre, Centraalbureau voor Schimmelcultures, Utrecht, The Netherlands) was used. The construction of the respective Δ*flo8* mutant and the VHH-secreting strain has been described elsewhere [21, 25]. Strain propagation was routinely done on YPD agar plates at 30 °C for 48 h. As precultures for bioreactor cultivations, 100 mL of YPD liquid media in a 1 L shake flask were inoculated with a cryo vial of the respective strain and incubated overnight at 25 °C and 180 rpm on a rotary shaker. YPD solid and liquid media contained per liter 20.0 g of soy peptone, 10.0 g of yeast extract, 20 g of glucose, and, in the case of solid media, 20 g of agar–agar. If appropriate, Zeocin was added to the media at 50 μg L^{-1}.

Bioreactor cultivations

Aerobic, glucose-limited, chemostat cultivations for the determination of the strain-specific growth parameters and q_P-to-μ ratios were carried out in 1.8 L parallel benchtop bioreactors (Eppendorf, Germany) at 7 distinct dilution rate setpoints, reaching from 0.015 to 0.170 h^{-1}. Two dilution rate setpoints were analyzed per individual chemostat cultivation. Samples were taken after seven volume changes had passed at a respective dilution rate. Precultures were grown as described above, harvested, washed, and resuspended in chemostat media, and used to inoculate the prefilled bioreactors to an OD_{600} of 0.2. Chemostat cultures were operated at a working volume of 0.6 L, except for chemostats preceding the retentostat phase as well as an additional set of chemostats carried out at a dilution rate of 0.1 h^{-1}, where the working volume was 1.4 L. The working volume was kept steady using a level sensor. Reactors were stirred at a constant rate of 700 rpm and aerated at a constant airflow of 0.5 L min^{-1}. The dissolved oxygen (DO) was monitored with a DO probe and controlled at 30% throughout initial batch cultures. Throughout all chemostat and retentostat cultures, DO remained above 50%. Hence, adjusting the level of oxygenation was not necessary to ensure sufficient oxygen supply. The culture temperature was controlled at 30 °C, and the pH was kept at 5.0 by the automated addition of a 12.5% ammonia solution. Chemostat medium contained (per liter) 10 g glucose, 5 g $(NH_4)_2SO_4$, 3 g KH_2PO_4, 0.5 g $MgSO_4 \cdot 7H_2O$, 1.5 mL of trace metal solution [69], 0.8 mL of 0.1 g L^{-1} biotin solution (Sigma-Aldrich, USA), and 0.25 g Pluronic 6100 PE antifoaming agent (BASF, Germany).

Aerobic, glucose-limited retentostat cultivations were performed in a similar manner as described previously [21]. Briefly, retentostat cultures were initiated from steady-state chemostat cultures operated at $D = 0.025$ h^{-1} by switching the reactor effluent to an outflow port equipped with an autoclavable filter assembly (TRACE Analytics). By this, a perfusion rate of 0.025 h^{-1} was maintained throughout the retentostat phase. The bioreactor system, main culture conditions (aeration, pH, and temperature), as well as the medium composition (except for glucose), were as described above. Retentostats were operated at a working volume of 1.4 L To predict retentostat growth dynamics, the predictive biomass accumulation script of Rebnegger et al. [21] was used. The maintenance energy requirement (m_S), the maximum theoretical yield (Y_{XS}^{max}) and a linear function for the specific productivity (q_P) in relation to the specific

growth rate (μ) were deduced from the chemostat data as described below. According to the chosen feeding regime, the working volume of the mixing vessel (a redesignated 1.8 L Eppendorf benchtop bioreactor) was kept steady at 1.5 L by using a level sensor, and the glucose concentration in the media was gradually decreased from 10 to 3.5 g L^{-1} upon initiation of the retentostat phase. A schematic diagram of the retentostat setup is provided as Additional file 1: Fig. S7.

Viability measurement

Viability was determined based on propidium iodide staining. Briefly, samples were diluted with PBS to an OD_{600} of 0.5 and stained with propidium iodide stock solution to a final concentration of 2.0 μmol L^{-1}. Samples were then analyzed on a Cytoflex S (Beckman Coulter).

Biomass measurement

OD_{600} was measured on a lab photometer. Biomass concentration (yeast dry mass, YDM) was routinely determined in technical duplicates. For this purpose, 5 mL of culture broth was harvested by centrifugation at 4000 *g* for 5 min, washed twice with demineralized water, transferred to a pre-weighed beaker, and dried at 105 °C for at least 48 h.

Measurement of the recombinant protein

Quantification of the recombinant secreted protein in the supernatant and filtrate was done by microfluidic capillary employing the LabChip GX/GXII System (PerkinElmer). The consumables Protein Express Lab Chip (760499, PerkinElmer) and Protein Express Reagent Kit (CLS960008, PerkinElmer) were used. Chip and sample preparation were done according to the manufacturer's recommendations. Quantification was done by employing the LabChip software provided by the manufacturer. For protein gel analysis of culture supernatants, NuPAGE® Novex® 12% Bis–Tris gels and MOPS buffer were used according to the manufacturer's instructions. Proteins were visualized by silver staining as described in Heukeshoven and Dernick [70].

Calculations of m_S, $Y_{XS}{}^{max}$ and $Y_{PS}{}^{max}$ for retentostat growth predictions To determine how m_S and $Y_{XS}{}^{max}$ of the producing strain change with μ, q_S was determined at D = μ ranging from 0.015 to 0.170 h^{-1} in chemostat cultures, and regression analysis on moving windows of three q_S values calculated at three consecutive μ values was done. This analysis is based on the Pirt equation, where the intercept at the y-axis gives m_S and the reciprocal of the slope is $Y_{XS}{}^{max}$ [19, 30]. To fully solve the equation, the maximum theoretical product yield ($Y_{PS}{}^{max}$) needs to be known, which was calculated in COBRApy [71] by employing the *K. phaffii* genome-scale metabolic model, iMT1026v3 [32].

iMT1026v3 was constrained with a non-growth associated maintenance of 2.81 mmol ATP g^{-1} h^{-1} and a glucose uptake rate of 2.46 mmol g^{-1} h^{-1}. The oxygen and CO_2 exchange rates were unbounded. The reactions for the VHH production were introduced into iMT1026v3, accounting for amino acid polymerization and the associated energetic requirements (4.3 mmol ATP per mmol g^{-1} amino acid) according to [72]. $Y_{PS}{}^{max}$ was calculated at 0.609 g g^{-1} by maximizing the secretion reaction for the assembled VHH.

Retentostat non-linear regression analysis and estimation of specific productivity

Regression analysis of biomass accumulation in retentostats for the determination of m_S, q_S and μ was achieved by least-squares regression analysis employing a Python implementation of the model described in Rebnegger et al. [21]. A modification was made in the q_P-μ relationship; rather than assuming a constant linear relationship, a Gompertz equation was fitted to the determined q_P values (see below) and the μ values determined from point-wise interpolation of the C_X values in the retentostat, in addition to the q_P and μ of the separate chemostat cultivations. The fitted function was incorporated into the regression model (the updated model can be found at https://github.com/bcoltman/Kphaffii_NearZero) and used instead of the linear relationship described previously.

A piecewise product balance accounting for production, accumulation and washout was used to calculate q_P. To achieve this, the biomass (C_X) and measured product (C_{P_M}) concentrations were linearly interpolated between the sampling points at approx. 24-h intervals. The concentration of the product in the supernatant, if productivity was zero between time points (C_{P_0}), was calculated via Eq. 2, accounting for wash-out kinetics where ϕ is the perfusion rate.

$$C_{P\_0_i} = C_{P\_M_{i-1}} * e^{((t_i - t_{i-1})*-\varphi)} \qquad (2)$$

The concentration of de novo secreted product (C_{P_N}) within a given time period was calculated according to Eq. 3:

$$C_{P\_N_i} = C_{P\_M_i} - C_{P\_O_i} \qquad (3)$$

And q_P was calculated according to Eq. 4:

$$q_P = \frac{C_{P\_N_i}}{\left(\frac{C_{X_i} + C_{X_{i-1}}}{2}\right) * (t_i - t_{i-1})} \qquad (4)$$

HPLC analysis of sugars, organic acids, and alcohols

Mixing vessel samples, culture supernatants, and filtrates were analyzed on a high-performance liquid

chromatography (HPLC) setup (Shimadzu Corporation, Japan) equipped with a Rezex ROA-organic acid H+col-umn (300 mm by 7.8 mm; Phenomenex, USA). A refraction index detector (RID-10A; Shimadzu Corporation, Japan) was used for quantitation. The column was operated at 60 °C, the flow rate was set at 1 mL min^{-1}, and 4 mM H_2SO_4 served as the mobile phase. Before injection, 0.9 mL of sample were mixed with 0.1 mL of 40 mM H_2SO_4 and filtered through a 0.20-µm regenerated cellulose (RC) membrane filter. The injection volume was 10 µL.

Sample preparation for biomass composition analysis

Samples for biomass analysis were washed with cold deionized water, snap-frozen in liquid nitrogen, and stored at − 70 °C until further use. With the exception of biomass samples for lipidomics, samples were lyophilized before the respective analysis, and the lyophilized biomass was aliquoted into appropriate amounts into sealable glass vials using a microbalance.

Macromolecular biomass composition analysis Total carbohydrate content was determined based on the phenol method [73]. Briefly, 0.15 mg of lyophilized biomass were resuspended in 1 mL of deionized water and mixed with 1 mL of a 5% phenol solution. Afterwards, 5 mL of 96% sulfuric acid were added, and the solution was incubated for 45 min at room temperature. Subsequently, the absorbance was measured at 488 nm, using glucose solutions as a standard. Results were corrected for the presence of nucleic acid pentoses using a relative absorbance of 0.445 AU and 0.264 AU for RNA and DNA, respectively.

Storage carbohydrate content in the form of glycogen and trehalose was measured as described previously [21], with the exception that for quenching and washing of the pellet, a pre-cooled (− 20 °C) "low salt" (0.05 M NaCl) and "high pH" (0.125 M Tris HCl; pH 8.2) MeOH (60%) quenching solution was used instead of pure methanol [74].

Total RNA content was determined according to Benthin et al. [75]. Briefly, 4 mg of lyophilized biomass were resuspended in 1 mL of cold 0.7 M $HClO_4$. Subsequently, 950 µL of this suspension was transferred to a 15 mL polypropylene tube and mixed with 2050 µL of cold 0.7 M $HClO_4$. Afterwards, the biomass was centrifuged, washed twice with 3 mL of cold 0.7 M $HClO_4$ (4200 g for 10 min at 4 °C), and resuspended in 3 mL of 0.3 M KOH to lyse cells. The lysate was incubated at 37 °C for 1 h, and, after cooling, 1 mL of cold 3 M $HClO_4$ was added for neutralization, and the sample was centrifuged again. The supernatant was then transferred to a fresh polypropylene tube, and the extraction step was repeated two more times. The respective extracts were

pooled and centrifuged to remove $KClO_4$ precipitates before the absorbance was measured at 260 nm against a blank. The RNA quantity was calculated by assuming 1 unit of absorbance at 260 nm corresponds to 0.038 mg RNA mL^{-1} and considering sample dilution.

Total DNA content was analyzed by adapting the Schmidt-Thannhauser-Schneider method according to Herbert et al. [73]. Briefly, 2.5 mg of lyophilized biomass were treated in the same manner as for total RNA content analysis, with the exception that the whole procedure was downscaled to fit into 1.5 mL screw cap centrifugation tubes. After the RNA extraction was completed, the remaining pellet (containing the DNA) was resuspended in 1 mL of 0.5 M $HClO_4$, incubated for 15 min at 70 °C, and then centrifuged for 2 min at 12,000 g and 4 °C. The supernatant was collected in a fresh tube, and the DNA extraction step was repeated two more times using 0.25 mL of 0.5 M $HClO_4$. The DNA extracts were pooled, and the absorbance was measured at 260 nm against a blank. The DNA quantity was calculated by assuming 1 unit of absorbance at 260 nm corresponds to 0.050 mg DNA mL^{-1} and considering sample dilution.

The total protein content was measured by the Biuret method [73]. Briefly, 4 mg of lyophilized biomass were resuspended in 500 µL of deionized water. Samples were then split into two 250-µL aliquots and mixed with 125 µL of 3 M NaOH. Heat extraction was done for 5 min at 99 °C. Subsequently, 125 µL of a 2.5% $CuSO_4$ solution was added. Afterwards, the samples were centrifuged for 5 min at 12,000 g, and a 200 µL aliquot of the supernatant was transferred to a transparent 96-well plate. The absorbance was measured on a Tecan reader at 488 nm, using BSA solutions as standard.

Protein amino acid composition analysis

For amino acid analysis, approximately 3 mg of lyophilized cells were hydrolyzed, both using (1) HCl after prior oxidation of sulfur-containing amino acids and (2) using methanesulfonic acid for the analysis of unstable amino acids. Tryptophan is degraded in both hydrolysis methods and, hence, could not be quantified. As glutamine is converted to glutamate and asparagine to aspartate during hydrolysis, the sums of these pairs were evaluated (GlX and AsX, respectively). For the analysis of most amino acids, an automated sample preparation robot (MPS2, Gerstel) was used for just-in-time online derivatization with N-(tert butyldimethylsilyl)-N-methyltrifluoroacetamide with 1% tert butyldimethylchlorosilane prior to gas chromatography—tandem mass spectrometry measurements on a GC–MS/MS (7890B GC with 7010B triple quadrupole GC–MS, Agilent Technologies) equipped with a 5% diphenyl 95% dimethyl polysiloxane analytical GC column (30 m, 0.25 mm ID, 0.25 mm film

Rebnegger *et al. Microbial Cell Factories*   (2024) 23:43

Page 17 of 20

thickness, Phenomenex ZB5 MS; detailed column setup in Additional file 1). Two amino acids, namely arginine and histidine, were analyzed via LC–MS/MS on a HILIC column (XBridge Amide analytical column;150×2.1 mm, 3.5 μm particle size, Waters, Milford, USA). Data evaluation was based on external calibration and internal standardization (amino acid standards of certified purity and stability were used). The internal standard, a heavy isotope-labeled "Cell Free" Amino Acid Mix (U-13C, 97–99% & U-15 179 N, 97–99%, Cambridge Isotope Laboratories), was added to the samples prior to hydrolysis. For a detailed description of hydrolysis and GC–MS analysis, see Szeliová et al. [76] and for modifications of this method and the LC–MS/MS method, see Additional file 1.

Lipidomics Lipid class quantification followed the protocol of Schoeny et al. [77] applying a sample-matched ^{13}C-labeled internal standard (ISTD) [78] on reversed-phase liquid chromatography (RP-LC) coupled with high-resolution mass spectrometry (HRMS). In brief, a homogenous cell mixture of the samples and the ISTD was extracted via an adopted Folch protocol [79]. An Acquity HSS T3 (2.1 mm×150 mm, 1.8 μm, Waters) equipped with a VanGuard Pre-column (2.1×5 mm, 100 Å, 1.8 μm, Waters) was used on a Vanquish™ Horizon HPLC (Thermo Scientific) coupled to a high field Q Exactive HF quadrupole-Orbitrap mass spectrometer (Thermo Scientific). As eluents, acetonitrile (ACN)/H_2O (3:2, v/v) and IPA/ACN (9:1, v/v), both containing 0.1% formic acid and 10 mM ammonium formate, were used in a 30 min run. Lipid identification was performed with LipidSearch 4.2 from Thermo Scientific, and quantitative data processing was performed in R/R studio. A more detailed description is provided in Additional file 1.

RNA isolation and quantitative PCR

RNA was isolated from cell pellets from chemostat and retentostat cultivations using the Tri reagent according to the supplier's instructions (Ambion, USA). Cells were disrupted by glass beads using a ribolyser (MP Biomedicals). To remove residual DNA, the RNA samples were treated with the DNA-free™-kit (Ambion) according to the manufacturer's manual. Subsequently, RNA quality, purity, and concentration were analyzed by a NanoDrop™ spectrophotometer and Bioanalyzer (Agilent). For cDNA synthesis for qPCR, the Biozym cDNA synthesis kit (Biozym) in combination with oligo(dt)$_{23}$ primers (NEB) was used. Quantitative PCR was carried out using the Biozym Blue Probe qPCR kit on a Rotor Gene Q instrument (Qiagen). Changes in transcript levels were calculated relative to the reference sample after normalization to *ACT1* (PP7435_Chr3-0993) expression using the threshold cycle method of the Rotor Gene software.

A more detailed description and a list of the used primers is provided in Additional file 1.

RNA-Seq library preparation

Library generation and sequencing were performed at the Vienna Biocenter Core Facility NGS Unit (www.vbcf.ac.at). Ribosomal RNA was depleted from total RNA (NEB) using an in-house method. The resulting ribo-depleted RNA was then fragmented, and cDNA libraries were generated using the NEBNext® Ultra™ II Directional RNA Library Prep Kit for Illumina (NEB). Libraries were sequenced as paired-end 150-base pair reads on an Illumina NovaSeq 6000 using the SP workflow.

RNA-Seq analysis

The raw BAM files were merged and sorted using samtools 1.9 [80]. For trimming, cutadapt 1.18 [81] was used. Alignment was performed with BowTie2 2.3.5.1 [82, 83] against the reference sequence of *K. phaffii* CBS7435. As the count quantification with kallisto depends on a transcript index of the reference sequences, this index was created with kallisto index v0.46.0 [84] and the latest *K. phaffii* CBS7435 annotation (FR839628.1, FR839629.1, FR839630.1, FR839631.1, FR839632.1). Accordingly, the count data of all sample reads was calculated with kallisto quant v0.46.0. Differential expression analysis [85] for each sample comparison was performed with several R v4.0.3 packages, which are tximport v1.18.0 [86], readr v1.1.0 [87], and DESeq2 v1.30.0 [85, 88, 89].

Cluster and GO enrichment analysis

Differentially expressed genes were grouped according to their expression profiles by the Genesis software tool [90], employing *k*-means clustering. According to figure-of-merit analysis, a *k* value of 4 was determined to be the ideal number of clusters for the data set. For the determination of enriched Gene Ontology (GO) terms in the respective clusters, the online Generic GO Term Finder tool (http://go.princeton.edu/cgi-bin/GOTermFinder) and *Saccharomyces* Genome Database (SGD) annotations were used. The cut-off for the corrected *p*-value (Bonferroni correction) was set to 0.05, and a *K. phaffii*-specific background list comprised of all annotated genes and genes with unknown function was provided.

Supplementary Information

> **Additional file 1:.** Additional Figures and Tables as well as additional Materials and Methods.
>
> **Additional file 2.** Detailed biomass composition measurement data for triplicate chemostat and retentostat cultivations, clusters identified by *k*-means cluster analysis and corresponding enriched GO terms as well as

Rebnegger *et al. Microbial Cell Factories*   (2024) 23:43

Page 18 of 20

Log$_2$ FC data and adjusted *p*-values for *K. phaffii* genes with a role in lipid biosynthesis.

Author contributions
CR, DM and BG contributed to study conception and design and data analysis. DP adapted the MATLAB code for growth predictions and performed metabolic modelling. Bioreactor cultivations and corresponding measurements were performed by CR and VK. BC adapted and transferred the non-linear regression model to Python and performed the analysis. Macromolecular and storage carbohydrate content measurements as well as RNA isolation for RNA-Seq were done by CR and VK. Amino acid analysis was done by CT and SH. Lipid analysis was performed by HS and GK. Elemental biomass composition was analyzed by AM. Funding was acquired by BG. The manuscript was written by CR and reviewed by BC, HS, CT, DM and BG. All authors read and approved the final manuscript.

Availability of data and materials
All data are included in the manuscript or its supplements. The regression model and its associated data and results are available at https://github.com/bcoltman/Kphaffii_NearZero. RNA-Seq raw data was deposited at NCBI SRA with the accession ID PRJNA1013119.

Declarations

Competing interests
The authors declare no competing interests.

Author details
[1]CD-Laboratory for Growth-Decoupled Protein Production in Yeast at Department of Biotechnology, University of Natural Resources and Life Sciences (BOKU), Vienna, Austria. [2]Department of Biotechnology, Institute of Microbiology and Microbial Biotechnology (IMMB), University of Natural Resources and Life Sciences, Vienna, Muthgasse 18, 1190 Vienna, Austria. [3]Austrian Centre of Industrial Biotechnology (ACIB GmbH), Muthgasse 11, 1190 Vienna, Austria. [4]Department of Forest- and Soil Sciences, Institute of Soil Research, University of Natural Resources and Life Sciences, Vienna, Peter-Jordan-Straße 82, 1190 Vienna, Austria. [5]Department of Chemistry, Institute of Analytical Chemistry, University of Natural Resources and Life Sciences, Vienna, Muthgasse 18, 1190 Vienna, Austria. [6]Department of Analytical Chemistry, Faculty of Chemistry, University of Vienna, Waehringer Straße 38, 1090 Vienna, Austria. [7]Vienna Metabolomics Center (VIME), University of Vienna, Althanstraße 14, 1090 Vienna, Austria.

References
1. Walsh G, Walsh E. Biopharmaceutical benchmarks 2022. Nat Biotechnol. 2022;40:1722–60.
2. Tripathi NK, Shrivastava A. Recent developments in bioprocessing of recombinant proteins: expression hosts and process development. Front Bioeng Biotechnol. 2019;7:420.
3. Vieira Gomes AM, Souza Carmo T, Silva Carvalho L, Mendonca Bahia F, Parachin NS. Comparison of yeasts as hosts for recombinant protein production. Microorganisms. 2018;6:38.
4. Rettenbacher LA, Arauzo-Aguilera K, Buscajoni L, Castillo-Corujo A, Ferrero-Bordera B, Kostopoulou A, Moran-Torres R, Núñez-Nepomuceno D, Öktem A, et al. Microbial protein cell factories fight back? Trend Biotechnol. 2021;40:576–90.
5. Peebo K, Neubauer P. Application of continuous culture methods to recombinant protein production in microorganisms. Microorganisms. 2018;6:56.
6. Looser V, Bruhlmann B, Bumbak F, Stenger C, Costa M, Camattari A, Fotiadis D, Kovar K. Cultivation strategies to enhance productivity of *Pichia pastoris*: a review. Biotechnol Adv. 2015;33:1177–93.
7. Regenberg B, Grotkjaer T, Winther O, Fausboll A, Akesson M, Bro C, Hansen LK, Brunak S, Nielsen J. Growth-rate regulated genes have profound impact on interpretation of transcriptome profiling in *Saccharomyces cerevisiae*. Genome Biol. 2006;7:R107.
8. Castrillo JI, Zeef LA, Hoyle DC, Zhang N, Hayes A, Gardner DC, Cornell MJ, Petty J, Hakes L, Wardleworth L, et al. Growth control of the eukaryote cell: a systems biology study in yeast. J Biol. 2007;6:4.
9. Gutteridge A, Pir P, Castrillo JI, Charles PD, Lilley KS, Oliver SG. Nutrient control of eukaryote cell growth: a systems biology study in yeast. BMC Biol. 2010;8:68.
10. Rebnegger C, Graf AB, Valli M, Steiger MG, Gasser B, Maurer M, Mattanovich D. In *Pichia pastoris*, growth rate regulates protein synthesis and secretion, mating and stress response. Biotechnol J. 2014;9:511–25.
11. Kumar K, Venkatraman V, Bruheim P. Adaptation of central metabolite pools to variations in growth rate and cultivation conditions in *Saccharomyces cerevisiae*. Microb Cell Fact. 2021;20:64.
12. Xia J, Sánchez BJ, Chen Y, Campbell K, Kasvandik S, Nielsen J. Proteome allocations change linearly with the specific growth rate of *Saccharomyces cerevisiae* under glucose limitation. Nat Commun. 2022;13:2819.
13. Liu Z, Hou J, Martinez JL, Petranovic D, Nielsen J. Correlation of cell growth and heterologous protein production by *Saccharomyces cerevisiae*. Appl Microbiol Biotechnol. 2013;97:8955–62.
14. Maccani A, Landes N, Stadlmayr G, Maresch D, Leitner C, Maurer M, Gasser B, Ernst W, Kunert R, Mattanovich D. *Pichia pastoris* secretes recombinant proteins less efficiently than Chinese hamster ovary cells but allows higher space-time yields for less complex proteins. Biotechnol J. 2014;9:526–37.
15. Hensing M, Rouwenhorst R, Heijnen J, van Dijken J, Pronk J. Physiological and technological aspects of large-scale heterologous-protein production with yeasts. Antonie Van Leeuwenhoek. 1995;67:261–79.
16. Porro D, Sauer M, Branduardi P, Mattanovich D. Recombinant protein production in yeasts. Mol Biotechnol. 2005;31:245–59.
17. Liu Y, Esen O, Pronk JT, van Gulik WM. Uncoupling growth and succinic acid production in an industrial *Saccharomyces cerevisiae* strain. Biotechnol Bioeng. 2021;118:1576–86.
18. Dierickx S, Maes K, Roelants S, Pomian B, Van Meulebroek L, De Maeseneire SL, Vanhaecke L, Soetaert WK. A multi-omics study to boost continuous bolaform sophorolipid production. N Biotechnol. 2022;66:107–15.
19. Ercan O, Bisschops MM, Overkamp W, Jorgensen TR, Ram AF, Smid EJ, Pronk JT, Kuipers OP, Daran-Lapujade P, Kleerebezem M. Physiological and transcriptional responses of different industrial microbes at near-zero specific growth rates. Appl Environ Microbiol. 2015;81:5662–70.

20. Wanka F, Arentshorst M, Cairns TC, Jørgensen T, Ram AF, Meyer V. Highly active promoters and native secretion signals for protein production during extremely low growth rates in *Aspergillus niger*. Microb Cell Fact. 2016;15:145.

21. Rebnegger C, Vos T, Graf AB, Valli M, Pronk JT, Daran-Lapujade P, Mattanovich D. *Pichia pastoris* exhibits high viability and a low maintenance energy requirement at near-zero specific growth rates. Appl Environ Microbiol. 2016;82:4570–83.

22. Juergens H, Hakkaart XDV, Bras JE, Vente A, Wu L, Benjamin KR, Pronk JT, Daran-Lapujade P, Mans R. Contribution of Complex I NADH dehydrogenase to respiratory energy coupling in glucose-grown cultures of *Ogataea parapolymorpha*. Appl Environ Microbiol. 2020;86:e00678–20.

23. Vos T, Hakkaart X, van Maris A, Pronk J, Daran-Lapujade P. *Saccharomyces cerevisiae* is extremely robust and maintains high metabolic capacity at aerobic near zero-growth rates. Microb Cell Fact. 2016;15:11.

24. De S, Rebnegger C, Moser J, Tatto N, Graf AB, Mattanovich D, Gasser B. Pseudohyphal differentiation in *Komagataella phaffii*: investigating the FLO gene family. FEMS Yeast Res. 2020;20:foaa044.

25. Gasser B, Rebnegger C, Flores Villegas MC, Mattanovich D. Carbon-source regulated protein production in a recombinant host cell. 2020, US Patent US11773424B2

26. Prielhofer R, Reichinger M, Wagner N, Claes K, Kiziak C, Gasser B, Mattanovich D. Superior protein titers in half the fermentation time: promoter and process engineering for the glucose-regulated *GTH1* promoter of *Pichia pastoris*. Biotechnol Bioeng. 2018;115:2479–88.

27. Van den Abbeele A, De Clercq S, De Ganck A, De Corte V, Van Loo B, Soror SH, Srinivasan V, Steyaert J, Vandekerckhove J, Gettemans J. A llama-derived gelsolin single-domain antibody blocks gelsolin-G-actin interaction. Cell Mol Life Sci. 2010;67:1519–35.

28. Zahrl RJ, Prielhofer R, Burgard J, Mattanovich D, Gasser B. Synthetic activation of yeast stress response improves secretion of recombinant proteins. N Biotechnol. 2023;73:19–28.

29. Maurer M, Kühleitner M, Gasser B, Mattanovich D. Versatile modeling and optimization of fed batch processes for the production of secreted heterologous proteins with *Pichia pastoris*. Microb Cell Fact. 2006;5:37.

30. Pirt SJ. The maintenance energy of bacteria in growing cultures. Proc R Soc Lond B Biol Sci. 1965;163:224–31.

31. Pirt SJ. Maintenance energy: a general model for energy-limited and energy-sufficient growth. Arch Microbiol. 1982;133:300–2.

32. Tomas-Gamisans M, Ferrer P, Albiol J. Fine-tuning the *P. pastoris* iMT1026 genome-scale metabolic model for improved prediction of growth on methanol or glycerol as sole carbon sources. Microb Biotechnol. 2018;11:224–37.

33. Mattanovich D, Gasser B, Prielhofer R. Constitutive promoter. 2013, US Patent US20140274761.

34. Cankorur-Cetinkaya A, Narraidoo N, Kasavi C, Slater NKH, Archer DB, Oliver SG. Process development for the continuous production of heterologous proteins by the industrial yeast, *Komagataella phaffii*. Biotechnol Bioeng. 2018;115:2962–73.

35. Lange HC, Heijnen JJ. Statistical reconciliation of the elemental and molecular biomass composition of *Saccharomyces cerevisiae*. Biotechnol Bioeng. 2001;75:334–44.

36. Jordà J, de Jesus SS, Peltier S, Ferrer P, Albiol J. Metabolic flux analysis of recombinant *Pichia pastoris* growing on different glycerol/methanol mixtures by iterative fitting of NMR-derived (13)C-labelling data from proteinogenic amino acids. N Biotechnol. 2014;31:120–32.

37. Liu Y, El Masoudi A, Pronk JT, van Gulik WM. Quantitative physiology of non-energy-limited retentostat cultures of *Saccharomyces cerevisiae* at near-zero specific growth rates. Appl Environ Microbiol. 2019;85:e01161-e11119.

38. Klose C, Surma MA, Gerl MJ, Meyenhofer F, Shevchenko A, Simons K. Flexibility of a eukaryotic lipidome—insights from yeast lipidomics. PLoS ONE. 2012;7: e35063.

39. Rußmayer H, Buchetics M, Gruber C, Valli M, Grillitsch K, Modarres G, Guerrasio R, Klavins K, Neubauer S, Drexler H, et al. Systems-level organization of yeast methylotrophic lifestyle. BMC Biol. 2015;13:80.

40. Adelantado N, Tarazona P, Grillitsch K, García-Ortega X, Monforte S, Valero F, Feussner I, Daum G, Ferrer P. The effect of hypoxia on the lipidome of recombinant *Pichia pastoris*. Microb Cell Fact. 2017;16:86.

41. Liu Z, Yu K, Wu S, Weng X, Luo S, Zeng M, Wang X, Hu X. Comparative lipidomics of methanol induced *Pichia pastoris* cells at different culture phases uncovers the diversity and variability of lipids. Enzyme Microb Technol. 2022;160: 110090.

42. Johnston EJ, Moses T, Rosser SJ. The wide-ranging phenotypes of ergosterol biosynthesis mutants, and implications for microbial cell factories. Yeast. 2020;37:27–44.

43. Dufourc EJ. Sterols and membrane dynamics. J Chem Biol. 2008;1:63–77.

44. Baumann K, Carnicer M, Dragosits M, Graf AB, Stadlmann J, Jouhten P, Maaheimo H, Gasser B, Albiol J, Mattanovich D, Ferrer P. A multi-level study of recombinant *Pichia pastoris* in different oxygen conditions. BMC Syst Biol. 2010;4:141.

45. Wang CW. Lipid droplet dynamics in budding yeast. Cell Mol Life Sci. 2015;72:2677–95.

46. Welte MA, Gould AP. Lipid droplet functions beyond energy storage. Biochim Biophys Acta Mol Cell Biol Lipids. 2017;1862:1260–72.

47. Kohlwein SD, Veenhuis M, van der Klei IJ. Lipid droplets and peroxisomes: key players in cellular lipid homeostasis or a matter of fat—store 'em up or burn 'em down. Genetics. 2013;193:1–50.

48. Ivashov VA, Grillitsch K, Koefeler H, Leitner E, Baeumlisberger D, Karas M, Daum G. Lipidome and proteome of lipid droplets from the methylotrophic yeast *Pichia pastoris*. Biochim Biophys Acta. 2013;1831:282–90.

49. Henne WM, Reese ML, Goodman JM. The assembly of lipid droplets and their roles in challenged cells. Embo j. 2018;37: e98947.

50. Spellman PT, Sherlock G, Zhang MQ, Iyer VR, Anders K, Eisen MB, Brown PO, Botstein D, Futcher B. Comprehensive identification of cell cycle-regulated genes of the yeast *Saccharomyces cerevisiae* by microarray hybridization. Mol Biol Cell. 1998;9:3273–97.

51. Ivashov VA, Zellnig G, Grillitsch K, Daum G. Identification of triacylglycerol and steryl ester synthases of the methylotrophic yeast *Pichia pastoris*. Biochim Biophys Acta. 2013;1831:1158–66.

52. Wriessnegger T, Sunga AJ, Cregg JM, Daum G. Identification of phosphatidylserine decarboxylases 1 and 2 from *Pichia pastoris*. FEMS Yeast Res. 2009;9:911–22.

53. Cox KH, Tate JJ, Cooper TG. Cytoplasmic compartmentation of Gln3 during nitrogen catabolite repression and the mechanism of its nuclear localization during carbon starvation in *Saccharomyces cerevisiae*. J Biol Chem. 2002;277:37559–66.

54. Egli T. How to live at very low substrate concentration. Water Res. 2010;44:4826–37.

55. Madhavan A, Arun KB, Sindhu R, Krishnamoorthy J, Reshmy R, Sirohi R, Pugazhendi A, Awasthi MK, Szakacs G, Binod P. Customized yeast cell factories for biopharmaceuticals: from cell engineering to process scale up. Microb Cell Fact. 2021;20:124.

56. Raschmanová H, Weninger A, Knejzlík Z, Melzoch K, Kovar K. Engineering of the unfolded protein response pathway in *Pichia pastoris*: enhancing production of secreted recombinant proteins. Appl Microbiol Biotechnol. 2021;105:4397–414.

57. Zahrl RJ, Gasser B, Mattanovich D, Ferrer P. Detection and elimination of cellular bottlenecks in protein-producing yeasts. Methods Mol Biol. 2019;1923:75–95.

58. Zavec D, Gasser B, Mattanovich D. Characterization of methanol utilization negative *Pichia pastoris* for secreted protein production: new cultivation strategies for current and future applications. Biotechnol Bioeng. 2020;117:1394–405.

59. Couderc R, Baratti J. Oxidation of methanol by the yeast, *Pichia pastoris*. Purification and properties of the alcohol oxidase. Agric Biol Chem. 1980;44:2279–89.

60. Staudacher J, Rebnegger C, Gasser B. Treatment with surfactants enables quantification of translational activity by O-propargyl-puromycin labelling in yeast. BMC Microbiol. 2021;21:120.

61. Carnicer M, Baumann K, Töplitz I, Sánchez-Ferrando F, Mattanovich D, Ferrer P, Albiol J. Macromolecular and elemental composition analysis and extracellular metabolite balances of *Pichia pastoris* growing at different oxygen levels. Microb Cell Fact. 2009;8:65.

62. Hoofnagle AN, Whiteaker JR, Carr SA, Kuhn E, Liu T, Massoni SA, Thomas SN, Townsend RR, Zimmerman LJ, Boja E, et al. Recommendations for the generation, quantification, storage, and handling of peptides used for mass spectrometry-based assays. Clin Chem. 2016;62:48–69.

63. Fountoulakis M, Lahm HW. Hydrolysis and amino acid composition of proteins. J Chromatogr A. 1998;826:109–34.

64. Jordà J, Jouhten P, Camara E, Maaheimo H, Albiol J, Ferrer P. Metabolic flux profiling of recombinant protein secreting *Pichia pastoris* growing on glucose:methanol mixtures. Microb Cell Fact. 2012;11:57.
65. Grillitsch K, Tarazona P, Klug L, Wriessnegger T, Zellnig G, Leitner E, Feussner I, Daum G. Isolation and characterization of the plasma membrane from the yeast *Pichia pastoris*. Biochim Biophys Acta. 2014;1838:1889–97.
66. Klug L, Daum G. Yeast lipid metabolism at a glance. FEMS Yeast Res. 2014;14:369–88.
67. Coltman BL, Rebnegger C, Gasser B, Zanghellini J. Characterising the metabolic rewiring of extremely slow growing *Komagataella phaffii*. Microb Biotechnol. 2024;17:e14386.
68. Zahrl R, Prielhofer R, Ata Ö, Baumann K, Mattanovich D, Gasser B. Pushing and pulling proteins into the yeast secretory pathway enhances recombinant protein secretion. Metab Eng. 2022;74:36–48.
69. Verduyn C, Postma E, Scheffers WA, Van Dijken JP. Effect of benzoic acid on metabolic fluxes in yeasts: a continuous-culture study on the regulation of respiration and alcoholic fermentation. Yeast. 1992;8:501–17.
70. Heukeshoven J, Dernick R. Simplified method for silver staining of proteins in polyacrylamide gels and the mechanism of silver staining. Electrophoresis. 1985;6:103–12.
71. Ebrahim A, Lerman JA, Palsson BO, Hyduke DR. COBRApy: COnstraints-based reconstruction and analysis for Python. BMC Syst Biol. 2013;7:74.
72. Stephanopoulos GN, Aristidou AA, Nielsen J. The essence of metabolic engineering. In: Metabolic engineering. Amsterdam: Elsevier; 1998. p. 1–20. https://doi.org/10.1016/B978-012666260-3/50002-9.
73. Herbert D, Phipps PJ, Strange RE. Chapter III chemical analysis of microbial cells. In: Norris JR, Ribbons DW, editors. Methods in microbiology, vol. 5. Cambridge: Academic Press; 1971. p. 209–344.
74. Mattanovich M, Russmayer H, Scharl-Hirsch T, Puxbaum V, Burgard J, Mattanovich D, Hann S. Metabolomics of *Pichia pastoris*: impact of buffering conditions on the kinetics and nature of metabolite loss during quenching. FEMS Yeast Res. 2017. https://doi.org/10.1093/femsyr/fox016.
75. Benthin S, Nielsen J, Villadsen J. A simple and reliable method for the determination of cellular RNA content. Biotechnol Tech. 1991;5:39–42.
76. Széliová D, Schoeny H, Knez Š, Troyer C, Coman C, Rampler E, Koellensperger G, Ahrends R, Hann S, Borth N, et al. Robust analytical methods for the accurate quantification of the total biomass composition of mammalian cells. Methods Mol Biol. 2020;2088:119–60.
77. Schoeny H, Rampler E, El Abiead Y, Hildebrand F, Zach O, Hermann G, Koellensperger G. A combined flow injection/reversed-phase chromatography-high-resolution mass spectrometry workflow for accurate absolute lipid quantification with ^{13}C internal standards. Analyst. 2021;146:2591–9.
78. Rampler E, Coman C, Hermann G, Sickmann A, Ahrends R, Koellensperger G. LILY-lipidome isotope labeling of yeast: in vivo synthesis of ^{13}C labeled reference lipids for quantification by mass spectrometry. Analyst. 2017;142:1891–9.
79. Folch J, Lees M, Sloane Stanley GH. A simple method for the isolation and purification of total lipides from animal tissues. J Biol Chem. 1957;226:497–509.
80. Li H, Handsaker B, Wysoker A, Fennell T, Ruan J, Homer N, Marth G, Abecasis G, Durbin R. The sequence alignment/map format and SAMtools. Bioinformatics. 2009;25:2078–9.
81. Martin M. Cutadapt removes adapter sequences from high-throughput sequencing reads. EMBnetjournal. 2011;17:10.
82. Langmead B, Salzberg SL. Fast gapped-read alignment with Bowtie 2. Nat Methods. 2012;9:357–9.
83. Langmead B, Wilks C, Antonescu V, Charles R. Scaling read aligners to hundreds of threads on general-purpose processors. Bioinformatics. 2019;35:421–32.
84. Bray NL, Pimentel H, Melsted P, Pachter L. Near-optimal probabilistic RNA-seq quantification. Nat Biotechnol. 2016;34:525–7.
85. Love MI, Huber W, Anders S. Moderated estimation of fold change and dispersion for RNA-seq data with DESeq2. Genome Biol. 2014;15:550.
86. Soneson C, Love MI, Robinson MD. Differential analyses for RNA-seq: transcript-level estimates improve gene-level inferences. F1000Res. 2015;4:1521.
87. readr: Read Rectangular Text Data. http://readr.tidyverse.org/index.html.
88. Gentleman RC, Carey VJ, Bates DM, Bolstad B, Dettling M, Dudoit S, Ellis B, Gautier L, Ge Y, Gentry J, et al. Bioconductor: open software development for computational biology and bioinformatics. Genome Biol. 2004;5:R80.
89. Huber W, Carey VJ, Gentleman R, Anders S, Carlson M, Carvalho BS, Bravo HC, Davis S, Gatto L, Girke T, et al. Orchestrating high-throughput genomic analysis with bioconductor. Nat Methods. 2015;12:115–21.
90. Sturn A, Quackenbush J, Trajanoski Z. Genesis: cluster analysis of microarray data. Bioinformatics. 2002;18:207–8.

Publisher's Note